LAPPEENRANTA UNIVERSITY OF TECHNOLOGY
Faculty of Technology
Technomathematics and Technical Physics

Heli Nenonen

THE ROLE OF VAN DER WAALS INTERACTIONS IN THE CASE OF H_2 ADSORPTION ON RUTHENIUM (0001) SURFACE

Examiners: Professor Matti Alatalo
Docent Katariina Pussi

ABSTRACT

Lappeenranta University of Technology
Faculty of Technology
Technomathematics and Technical Physics

Heli Nenonen

The role of van der Waals interactions in the case of H_2 adsorption on ruthenium (0001) surface

Master's thesis

2012

55 pages, 23 figures and 5 tables.

Examiners: Professor Matti Alatalo
Docent Katariina Pussi

Keywords: H_2, Ru(0001), Van der Waals-Density Functional, Density Functional Theory, Adsorption

Computational material science with the Density Functional Theory (DFT) has recently gained a method for describing, for the first time the non local bonding *i.e.*, van der Waals (vdW) bonding. The newly proposed van der Waals-Density Functional (vdW-DF) is employed here to address the role of non local interactions in the case of H_2 adsorption on Ru(0001) surface. The later vdW-DF2 implementation with the DFT code VASP (Vienna Ab-initio Simulation Package) is used in this study. The motivation for studying H_2 adsorption on ruthenium surface arose from the interest to hydrogenation processes.

Potential energy surface (PES) plots are created for adsorption sites *top*, *bridge*, *fcc* and *hcp*, employing the vdW-DF2 functional. The vdW-DF yields 0.1 eV - 0.2 eV higher barriers for the dissociation of the H_2 molecule; the vdW-DF seems to bind the H_2 molecule more tightly together. Furthermore, at the *top* site, which is found to be the most reactive, the vdW functional suggests no entrance barrier or in any case smaller than 0.05 eV, whereas the corresponding calculation without the vdW-DF does. Ruthenium and H_2 are found to have the opposite behaviors with the vdW-DF; Ru lattice constants are overestimated while H_2 bond length is shorter. Also evaluation of the CPU time demand of the vdW-DF2 is done from the PES data. From *top* to *fcc* sites the vdW-DF computational time demand is larger by 4.77 % to 20.09 %, while at the *hcp* site it is slightly smaller.

Also the behavior of a few exchange correlation functionals is investigated along addressing the role of vdW-DF. Behavior of the different functionals is not consistent between the Ru lattice constants and H_2 bond lengths. It is thus difficult to determine the quality of a particular exchange correlation functional by comparing equilibrium separations of the different elements. By comparing PESs it would be computationally highly consuming.

TIIVISTELMÄ

Lappeenrannan teknillinen yliopisto
Teknillinen tiedekunta
Teknillinen fysiikka ja matematiikka

Heli Nenonen

Van der Waals-voimien vaikutus vetymolekyylin adsorptioon ruteniumin (0001) pinnalle

Diplomityö

2012

55 sivua, 23 kuvaa ja 5 taulukkoa.

Tarkastajat: Professori Matti Alatalo
Dosentti Katariina Pussi

Hakusanat: H_2, Ru(0001), Van der Waals-tiheysfunktionaali, Tiheysfunktionaaliteoria, Adsorptio

Matemaattinen materiaalimallinnus tiheysfunktionaaliteorian avulla on hiljattain saanut menetelmän, jonka avulla pystytään nyt ensimmäistä kertaa kuvaamaan ei-lokaalit sidokset eli van der Waals sidokset. Tässä työssä keskitytään tutkimaan van der Waals (vdW) voimien vaikutusta vetymolekyylin adsorptioon ruteniumin (0001) pinnalle käyttäen uutta van der Waals-tiheysfunktionaalimenetelmää. Mallinnuksessa käytetään uudempaa vdW-DF2-implementaatiota tiheysfunktionaaliteoriaan perustuvan VASP (Vienna Ab-initio Simulation Package) laskentaohjelman kanssa. Erityisesti vetymolekyylin adsorptiota ruteniumin pinnalle ajoi tutkimaan kiinnostus hydrogenaatioprosessiin.

Potentiaalienergiapintapiirrokset esitetään symmetrisille adsorptiopaikoille käyttäen vdW-DF2 funktionaalia. VdW-tiheysfunktionaali aiheuttaa 0.1 eV - 0.2 eV korkeammat energiavallit vetymolekyylin hajoamiselle; vdW-funktionaali näyttää sitovan vetymolekyylin tiukemmin kasaan. Ru-atomin kohdalla oleva adsorptiopaikka on reaktiivisin neljästä symmetrisestä paikasta. Käytettäessä van der Waals funktionaalia sisääntulossa ei ole energiavallia sillä paikalla tai se on joka tapauksessa pienempi kuin 0.05 eV, kun sitä vastoin ilman vdW-funktionaalia energiavalli selvästi muodostuu sisääntuloon. Rutenium ja vetymolekyyli käyttäytyvät päinvastaisesti vdW-funktionaalin kanssa; funktionaali yliarvioi ruteniumin hilavakiot, kun taas vetymolekyylin sidospituus pienenee. Lisäksi tässä työssä on tutkittu kuinka paljon laskenta-aikaa vdW-DF2 funktionaali vaatii käyttäen potentiaalienergiapintojen laskenta-aikoja. Muilla adsorptiopaikoilla laskenta-ajat ovat pidempiä vdW-DF2 funktionaalin kanssa, ollen 4.77 % ja 20.09 % välillä, kun sitä vastoin *hcp*-paikan laskenta-aika on hieman lyhyempi vdW-funktionaalin kanssa.

Van der Waals-voimien vaikutuksen tutkimisen ohella testataan lisäksi muutaman vaihto-korrelaatiofunktionaalin käyttäytymistä. Niiden käytös osoittautuu erilaiseksi katsottaessa vetymolekyylin sidospituutta ja ruteniumin hilavakioita. Näin ollen on vaikea sanoa mitään yksittäisen funktionaalin laadusta tutkimalla erilaisten alkuaineiden tasapainotiloja. Potentiaalienergiapintoja tutkimalla se olisi erittäin rasittavaa laskenta-ajallisesti.

PREFACE

This Master's Thesis has been done for Technomathematics and Technical Physics within the Faculty of Technology at Lappeenranta University of Technology.

First I want to acknowledge my supervisor Professor Matti Alatalo. I am grateful for the opportunity to do my master's thesis within Computational Modeling of Materials research group. I wish to thank Professor Alatalo for the patient guidance. I want to thank my supervisor M.Sc. Mikko Puisto for the important guidance and for the encouragement throughout the process. I want to thank also D.Sc. Matti Lahti and all the other members of the research group for the help and also for the supporting spirit.

I want to thank Professor Murzin and the Laboratory of Industrial Chemistry and Reaction Engineering at Åbo Akademi for their hospitality during my stay in Turku.

I would like to thank Docent Katariina Pussi for her role as the second examiner of this thesis.

I want to thank my parents and my sister for their support throughout my studentship in Lappeenranta. I am grateful for the financial support my parents have provided me over the years. I also want to thank all the friends that I have met during my student days. I am grateful for their companionship inside the school and especially for their friendship outside the university. Finally, special thanks go to Olli. I want to thank him for all the support he has given me during my studies and the final thesis and also for setting a good example for me.

Turku 3.10.2012
Heli Nenonen

CONTENTS

ABBREVIATIONS

DFT	Density Functional Theory
DOS	Density Of States
fcc	face centered cubic
GGA	Generalized Gradient Approximation
hcp	hexagonal close packed
LDA	Local Density Approximation
LDOS	Local Density Of States
PAW	Projector-Augmented Wave
PES	Potential Energy Surface
VASP	Vienna Ab-initio Simulation Package
vdW	van der Waals
vdW-DF	van der Waals-Density Functional

1 INTRODUCTION

Van der Waals (vdW) bonding has a fundamental role within many diverse occurrences, from geckos to surface science. Computational surface science has for the first time, a method to describe the non local bonding *i.e.*, van der Waals bonding. The recently proposed van der Waals-Density Functional (vdW-DF) [1, 2] describes the non local correlations, that were neglected before. The original Density Functional Theory (DFT) takes into account only the local types of bonding. The recently proposed vdW-DF has already awaken attention and shown a glimpse of its importance at least in some particular systems within computational material science [3–6].

Van der Waals-Density Functional seems to be important in adsorption processes, and especially in the adsorption of large molecular systems on a surface. However, there have been reports that the vdW-DF does not seem to have notable influence on intra molecular bonds, only on intermolecular bonds. [3, 4]

The motivation for studying especially H_2 adsorption on ruthenium surface arose from the interest to hydrogenation process. To be precise, the hydrogenation of sugars. Ruthenium was picked out as a promising catalyst substance. In order to get a comprehensive view of the hydrogenation process, it is important to obtain information of the atomic level phenomena of the process.

The DFT code VASP (Vienna Ab-initio Simulation Package) is used within this study to perform all calculations. The latest version of the code, VASP 5.2 [7–10] is employed. The new vdW-DF2 [2] implementation [11] to the VASP code is used to describe the non local interactions.

First in this study, the essential test calculations for ruthenium and H_2 are done. The underlying test calculations have to be rigorous, because errors in those calculations result in the accumulation of errors in further calculations. For this reason the test calculations should not be taken lightly in any research.

After the mandatory test calculations have been done, one can move on to studying the role of the non local van der Waals interactions in DFT calculations. This recently proposed truly non local addition to the Density Functional Theory has attracted a lot of attention. The examining of the role of the vdW-DF in *ab initio* calculations will be done within this study also. For a start, comparisons of Ru lattice constants and cohesive energies will be done between the vdW-DF calculations and plain DFT calculations. Also H_2

bond lengths are compared between the vdW-DF calculations and without employing the vdW implementation.

In addition to studying the role of the non local corrections as described above, a set of generalized gradient approximation (GGA) exchange correlation functionals are studied also. Alongside with the newly proposed van der Waals-Density Functional, a couple of new exchange correlation functionals, C09 [12] and PW86R [13, 14] are introduced by others. These are created to tackle some issues with the vdW-DF and older exchange functionals, that are seen as shortcomings. Within this study also three older commonly used GGA exchange correlation functionals are used -the original PBE exchange functional [15], revPBE functional [16] and PW86 functional [13].

Secondly, to study the role of the vdW-DF implementation, adsorption calculations are performed and potential energy surface (PES) plots are produced. The ultimate goals are the H_2 adsorption on Ru(0001) calculations and the PES plots. Important information on H_2 adsorption on Ru surface is obtained with these calculations. PES plots yield information about dissociation barriers, reaction channels and adsorption energies. Potential energy surface (PES) calculations are done to study the adsorption process and the importance of the non local correlations in the process. Also some evaluation of the effect of the exchange correlation functional is made here. All ruthenium (0001) surface high symmetry adsorption sites: *top*, *bridge*, *fcc* and *hcp* are considered within this study. Some H_2 on Ru(0001) PES plots have been determined before by Luppi *et al.*, but not with involving the vdW-DF [17]. Within this study also local density of states (LDOS) plots are created for the *top* adsorption site in addition to the PES plots.

Quite quickly, at the beginning of making this study a question arose of the speed of the vdW-DF implementation. Thus, by side of the PES calculations, evaluation of the CPU time demand of the vdW-DF is done. The PES calculations made with including the vdW-DF implementation of the VASP code are compared to the ones that are made without employing the implementation. The comparison of computational time demand is made between *top*, *bridge*, *fcc* and *hcp* adsorption sites individually.

2 BACKGROUND THEORY

The most important aspect within this study is the bonding that forms between atoms and molecules, especially the van der Waals bonding. The van der Waals bonding plays a crucial role in surface science. Bonding between atoms and molecules is discussed first up in this chapter. Next the basics of Density Functional Theory, that the computational code VASP is based upon is described in general detail. After this, the actual van der Waals-Density Functional is described. Then, some fore view to the GGA exchange correlation functional testing is given. In the end, the description of the potential energy surface, which is the central quantity in theoretical description of adsorption, is given.

2.1 Chemical and van der Waals bonding

In order to comprehend the behavior of materials, one has to understand the concepts of atomic bonding. Bonding describes the structures of molecules and solid materials. The understanding of the types of the different bonds gives a highly valuable aspect to the properties of the materials.

Three different types of chemical bonding are present in solids: ionic, covalent and metallic. Chemical bonding arises from the fundamental tendency of the elements towards stable electron configurations.

Ionic bond is found in compounds of both metallic and non metallic elements. Metallic elements can donate one or more electrons to non metallic elements and when this occurs, the elements become positively and negatively charged. The elements attract each other resulting from the different charges and form an ionic bond. This attraction between oppositely charged ions is called Coulombic. In fact, the ionic bond is sometimes called the Coulombic bond.

In covalent and metallic bonds the electrons are shared. In covalent bonding electrons are shared and thus the orbitals of the atoms overlap. The covalently bonded atoms form partly common orbitals. Electrons can be shared and a covalent bond established between two or more atoms. It is possible to have inter atomic bonds that are partially covalent and partially ionic bonds. In fact it is rare for a compound to have purely ionic or purely covalent bonds.

In metallic bonds the valence electrons are shared and form a homogeneous electron gas. The charges can move freely in the “sea“ of electrons around atom cores. This explains

why metals conduct charge and heat. In addition, chemical bonding implies giving, receiving or sharing electrons.

In physical bonding, no trading of electrons is present. Secondary, van der Waals, or physical bonding is much weaker than chemical bonding. The bond energy is typically the order of 0.1 eV/atom. Nonetheless the van der Waals bonding *i.e.*, physical bonding exists virtually in all atoms or molecules, but its presence may be obscured when chemical bonding is present. Van der Waals effect is a non local correlation effect, meaning that it is totally intermolecular. Charge fluctuations in one atom or molecule are correlated in a nearby atom or molecule. Thus van der Waals bonding arises from atomic or molecular dipoles.

There are three sources for the van der Waals forces. First, there can be permanent dipoles in some molecules, although the material is electrically neutral. Caused by the distortion of charge, such dipoles align with each other and result an attractive force. Second, the presence of a such permanent dipole will induce temporary distortion of charge in a nearby molecule. Third, even though molecules are not permanent dipoles, the electrons are mobile and at any instant the negative charge of the electrons is likely not to be coincide with the positive charge of the nuclei. Thus the fluctuations of electrons make molecules dipoles, that vary over time. These kind of temporary dipoles cannot align in a such a way that permanent dipoles do, but they induce nevertheless polarization into adjacent molecules. This is called London dispersion. These fluctuations in molecules are present even in the permanent type of dipoles, and contribute generally the largest amount of intermolecular forces of the three types.

Van der Waals interactions are important within molecules and in molecular adsorption to a surface. Figure 1 represents how the charge fluctuation is induced to a nearby atom or molecule.

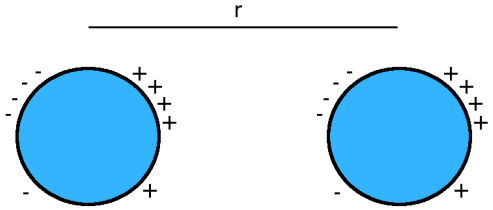

Figure 1: Schematic picture of van der Waals bonding between two atomic systems.

Fluctuation of electrons in atoms or molecules render dipoles and as a result, polarization is induced into adjacent atoms or molecules. Van der Waals effect is a non local correlation effect *i.e.*, it is totally intermolecular.

2.2 Density Functional Theory

The Density Functional Theory [18, 19] has been over the past 40 years an increasingly intriguing *ab initio* computational materials modeling method. The Latin term *ab initio* means from the beginning. In computational material science, the term *ab initio* refers to quantum mechanics and electronic structure methods. All *ab initio* methods are computationally heavy and expensive. The popularity of the DFT among *ab initio* methods is due to its relatively low computational cost compared to other *ab initio* methods. Nonetheless it can nowadays treat many material science problems with sufficiently high accuracy.

The first approximation that almost all *ab initio* methods encompass is the Born-Oppenheimer approximation. Since the core of an atom is three orders of magnitude heavier than the electrons, the electrons follow the movements of the core almost instantaneously. Giving this fact, the approximation of Max Born and Robert Oppenheimer states that in fact no finite relaxation time is needed by the electrons to follow the nuclear motion. And thus, solving the motion of the nucleus and the electrons are separated.

When considering systems of many electrons, solving the Schrödinger equation is no more feasible with any of the standard partial differential equation numerical solution methods. Approximations have to be made. The Density Functional Theory is one of the most popular methods for solving the ground state properties of atoms, molecules and solids.

The density functional theory began from suggestion of Hohenberg and Kohn in 1964 that a simple entity can be chosen for the basic variable: the electron density which minimizes the total energy. The many-body wave function and thus all properties of the system can be exactly defined by the electron density of the system. [18]

But if it would not have been for the *ansatz* suggested by Kohn and Sham in 1965, the density functional theory would have had only a shred of its popularity [19]. The *ansatz* (attempt in english) proposed that the complicated many-body effects are to be replaced by a simple exchange correlation functional. The Kohn-Sham approach, being a self-

consistent method, involves independent particles, but an interacting density. In the core of the *ansatz* lies the exchange correlation functional $E_{\text{xc}}[n]$. [19, 20]

Kohn and Sham proposed that the ground state energy could be written

$$E_{\text{KS}} = T_{\text{s}}[n] + \int \mathrm{d}\mathbf{r}\, V_{\text{ext}}(\mathbf{r})\, n(\mathbf{r}) + E_{\text{Hartree}}[n] + E_{\text{II}} + E_{\text{xc}}[n]. \tag{1}$$

Here $T_{\text{s}}[n]$ is the kinetic energy of the non-interacting electrons. $V_{\text{ext}}(\mathbf{r})$ is the external potential caused by the nuclei and other external fields (assumed to be independent of spin) and E_{II} is the interaction between the nuclei. $E_{\text{Hartree}}[n]$ is the classical Coulomb interaction energy of the electron density $n(\mathbf{r})$ interacting with itself. Finally, $E_{\text{xc}}[n]$ is the exchange correlation functional, that includes all the electron-electron interactions beyond the $E_{\text{Hartree}}[n]$ term. [19, 20]

The Kohn-Sham theorem is effective, because it separates the independent particle kinetic energy, the long-range Hartree terms and the exchange correlation functional $E_{\text{xc}}[n]$.

In the density functional theory, only the exchange correlation functional must be approximated. The approximation of the E_{xc} is also the main source of errors in DFT. Perhaps the most popular approximation these days, over the former local density and local spin density approximations, (LDA) and (LSDA), is the generalized gradient approximation. The GGA [21–24] further improved the accuracy of the DFT method, when it was introduced in the 80's.

2.3 New GGA exchange functionals

After the release of the new van der Waals-Density Functional (referred to as vdW-DF1 here) [1], and the second version of it (referred to as vdW-DF2 here) [2], some new exchange functionals have been proposed.

When proposing the second version of vdW-DF (vdW-DF2), Lee *et al.* preferred to use the exchange functional PW86R [13, 14]. In the same paper it is stated, that the revPBE exchange functional [16] can bind spuriously by exchange alone. The PW86R functional is built to offer consistently better agreement with Hartree-Fock calculations than the alternative functionals. In fact, that is the sole constructing criterion of the functional. However, there is no substantial difference to the PW86 functional [13], which was introduced in 1986. [14]

Also, a second new exchange functional, C09 [12] is introduced in the recent past. It is published with a comment that it may be suitable to be used with the original vdW-DF1 instead of the revPBE. C09 is proposed with the goal of remedying tendency of the vdW-DF1 to overestimate intermolecular distances. [12]

2.4 Van der Waals-Density Functional

The van der Waals interaction is a non local electron correlation effect. Chapter 2.1 gives an understanding of this effect. In DFT the correlation typically has local or semi-local nature. This general description dismisses the non local van der Waals interactions completely. Apropos, the recently introduced first principles van der Waals-Density Functional (vdW-DF) [1, 2] covers this shortcoming and takes into account the non local correlation between electrons.

The key to the vdW-DF method is to include the long range piece of the correlation energy, $E_c^{nl}[n]$. The electron correlation energy is now composed of two components, short- and long-range parts, $E_c[n] = E_c^0[n] + E_c^{nl}[n]$. The non local correlation energy $E_c^{nl}[n]$ is of the same form in both vdW-DF1 and vdW-DF2. It is written,

$$E_c^{nl}[n] = \int d^3r \int d^3r' n(\mathbf{r})\phi(\mathbf{r},\mathbf{r}')n(\mathbf{r}'). \tag{2}$$

The kernel ϕ is given as a function of $Rf(\mathbf{r})$ and $Rf(\mathbf{r}')$. Here $R = |\mathbf{r} - \mathbf{r}'|$ and $f(\mathbf{r})$ is a function of $n(\mathbf{r})$ and its gradient. In fact $f(\mathbf{r})$ is proportional to the exchange-correlation energy density ϵ_{xc} of a gradient corrected LDA at the point $\mathbf{r}$. [2]

The difference between the two vdW-DF's lies within the determining of the vdW kernel ϕ. The vdW-DF [1] described dispersion better than any other non empirical method before that, when it was published for general geometries in 2004. However, the older vdW-DF is said to overestimate equilibrium separations and to underestimate hydrogen bond strength. [2] The vdW-DF2 tackles these shortcomings. It substantially improves both, equilibrium separations and hydrogen bond strengths and furthermore it improves vdW attractions at intermediate separations longer than the equilibrium ones. [2]

There exists also other vdW methods within the DFT, for example the vdW-DF^{surf} [25], but those are not addressed here. The vdW-DF2 [2] is employed solely within this study.

2.5 Computational code VASP

VASP (Vienna Ab-initio Simulation Package) is an *ab initio* molecular dynamics computational code [7–10]. The VASP code is based on the Density Functional Theory (DFT). The code uses projector-augmented wave (PAW) method and a plane wave basis set to calculate the ground state properties of a system. [26, 27].

The projector augmented wave method (PAW) is an all-electron method for efficient *ab initio* molecular dynamics. The PAW combines traditions of the pseudopotential approach and the augmented wave methods into one electronic structure method. With the PAW method, transferability problems of the pseudopotential approach are avoided. [26, 28]

2.6 Adsorption and potential energy surface

The adsorption process is in the heart of surface science. Adsorption is generally classified to chemisorption and physiorption. Chemisorption implies true chemical bonding between the surface and the adsorbate whereas physical bonding refers to van der Waals bonding where no chemical bonding is present. The potential energy surface (PES) is the central quantity in theoretical description of adsorption. Creating a PES plot is the best way to get information about the reaction dynamics in a particular system.

The PES plots give information of the reaction barriers and the reaction channels. Potential energy surface plots are constructed by varying the bond length and the height of the molecule from the surface. The pairs of intermolecular bond length and the distance of the molecule from the surface are calculated in fixed points. Then the total energy of the system is plotted at these fixed points. Typically, neither the atoms in the molecule nor the surface atoms are allowed to move in the fixed points. As the surface atoms are declined to move, the calculation is called a frozen surface calculation. Some studies have been performed by others, to determine whether the frozen nature of the surface has an effect on the results of reaction barriers and reaction channels. No radical change was yielded to the PES plot, although the surface atoms were allowed to move [29]. The frozen surface method is the characteristic way to do PES calculations, and it is applied here also. A contour plot is the most informative way to present the PES calculation results. One contour line marks a change of 0.1 eV in the total energy. There exists a method called the Nudged Elastic Band (NEB), that would yield more precise information of the minimum energy path. The potential energy surface would be more delicate with the NEB, but it is not needed. The regular PES construction and the 0.1 eV contouring is fully sufficient and will be employed here. PES calculations are computationally very costly. About 65-90

calculation points are used to create one PES plot. An illustrative presentation of a PES plot is presented in figure 2.

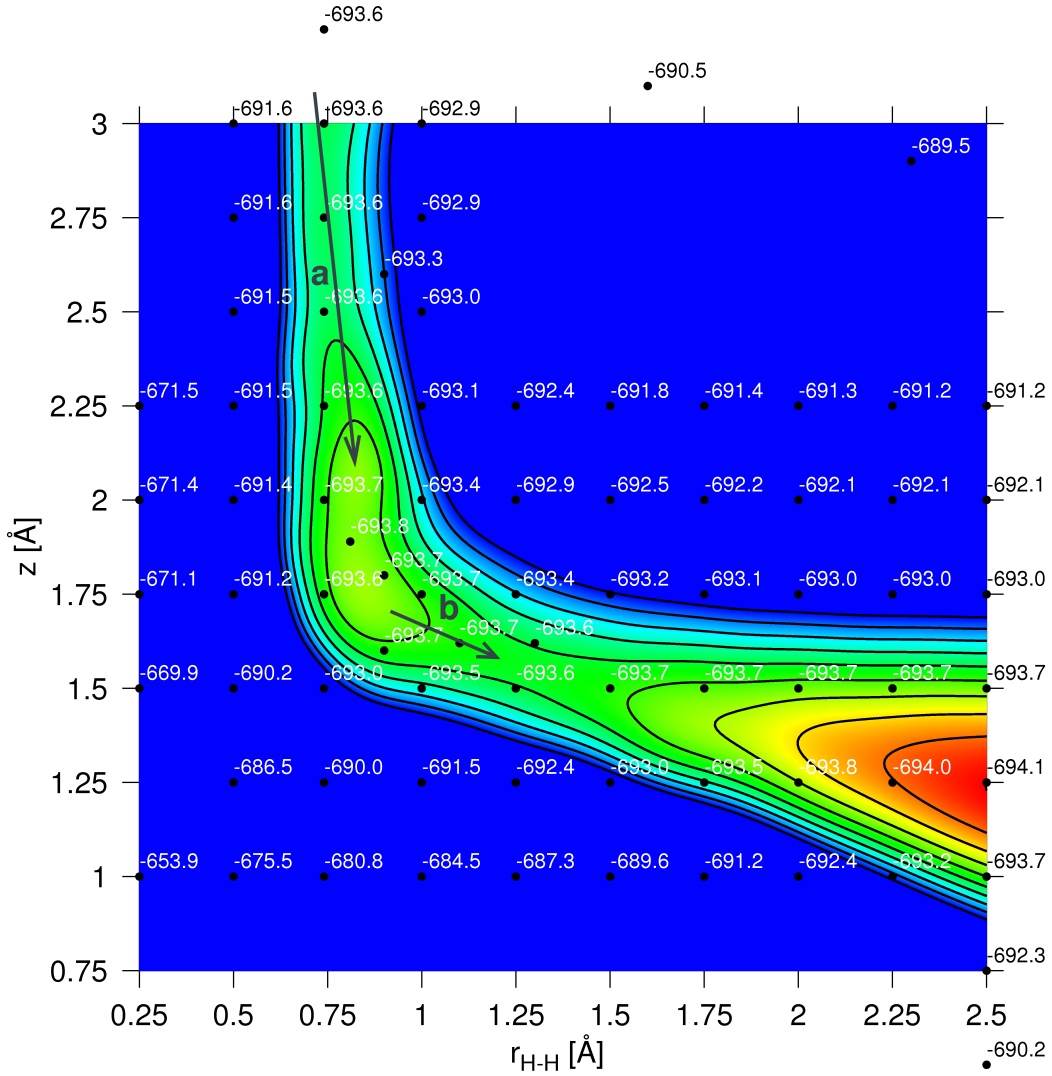

Figure 2: A typical PES plot. z denotes the distance between the surface and the molecule. $r_{\text{H-H}}$ denotes the bond length of the molecule. The contour spacing is 0.1 eV. The entrance channel is denoted by a and b denotes the dissociation channel.

The calculated fixed data points are plotted to the figure to get a view of how the PES plots are drawn. More inspection points are distributed around the reaction channel in the plot, and only a couple of checking points exist far away from the reaction channels. Notice, that a couple of points are bordered out from the figure although all the data points have been used to plot the surface image and the contours. The contour lines are drawn in a fixed spacing, and therefore it is easy to see for example the height of the dissociation barrier straight away from the figure. In this case the dissociation barrier is quite shallow, only 0.1 eV (see channel b in the figure above). The surface is attractive at this adsorption site (see channel a in the figure above), and the adsorption energy is 0.2 eV. One has to

bear in mind that even though the surface is attractive at a certain adsorption site, the reaction channel is different at other sites and even at the same site with other orientations of the molecule.

3 RESULTS

In the first section of this chapter, parameter testing is discussed. This has to be done before any further calculations with the VASP code, and before ultimately the main goal, potential energy surface (PES) calculations, can be done. The second section is about testing the vdW functional and some GGA exchange correlation functionals. Within these calculations, hydrogen molecule and ruthenium are in focus. The third section then focuses on H_2 adsorption on Ru(0001) surface. After determining the properties of a suitable surface slab, the PES plots are created of the H_2 adsorption on Ru(0001) surface at the *top*, *bridge*, *fcc* and *hcp* sites. Furthermore, local density of states (LDOS) plots are created for the *top* adsorption site. In the very end, after the PES calculations are done, some evaluation of the CPU time demand of the vdW-DF2 implementation is done.

Latest version of the VASP-code (VASP 5.2) [7–10] is used here for all calculations. Also the new vdW-DF2 [2] implementation [11] of the VASP code is employed in this study solely. (Whenever referred to vdW-DF in the results section, is referred precisely to the vdW-DF2.)

3.1 Test calculations for ruthenium and H_2

Calculations begin by determining the cut-off energies for Ruthenium and H_2. Also the lattice constants for ruthenium and the bond length and vacuum size for H_2 have to be determined in the beginning of computational calculations. Throughout the calculations in this study the vdW-DF2 [2] method was used, because it is more efficient compared to the older vdW-DF1 method [1].

3.1.1 Ruthenium cut-off energy

The cut-off energy should be chosen carefully, because it has a big influence on the accuracy of the calculations. Plane waves with a smaller kinetic energy than the chosen cut-off energy are included in the plane wave basis set. The bigger the cut-off, the more accurate the result. Consequently, the bigger the cut-off, the bigger the computational cost of calculation. The cut-off energy is a critical quantity within both the accuracy and the computational cost.

When dealing with elements that have a hexagonal crystal structure, a gamma centered k-point grid is highly recommended. Energy is known to converge much faster with

the gamma centered grids, than with the Monkhorst Pack grids. In fact, the standard Monkhorst Pack grids do not have full hexagonal symmetry. [30] Ruthenium has a hexagonal close packed crystal structure and therefore a 6×6×6 gamma centered k-point grid is used in these calculations. The exchange functional used here is the original PBE [15]. See figure 3 for a proper cut-off energy determined for ruthenium.

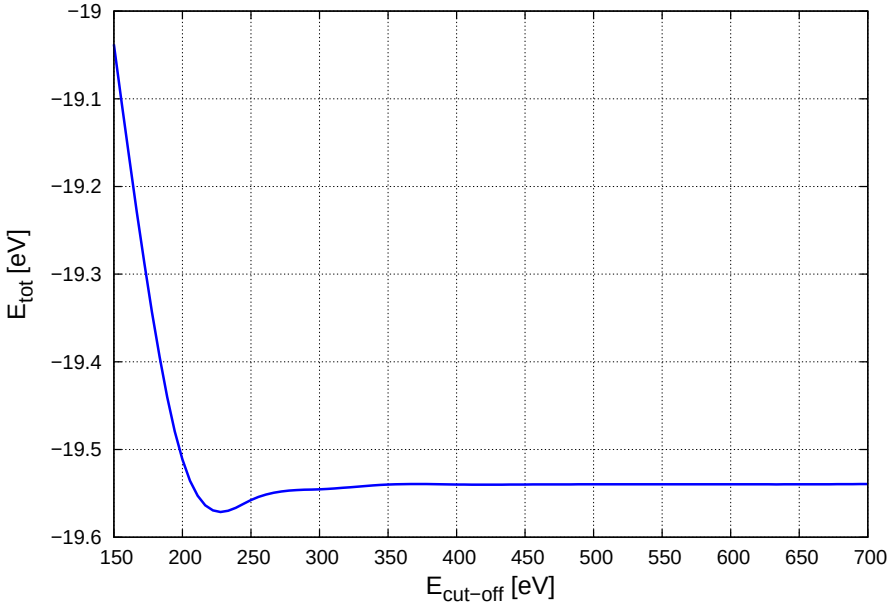

Figure 3: Total energy as a function of cut-off energy for ruthenium.

The cut-off energy is adequate when the curve of the total energy of the system flattens. The vdW-DF2 implementation does not have a substantial effect to the cut-off energy. The same cut-off energy can be chosen for the vdW-DF2 implementation calculation, and a calculation without the implementation. A cut-off energy of 400 eV is chosen for further calculations.

3.1.2 H_2 cut-off energy

Cut-off energy for the hydrogen molecule is determined before further calculations. In the case of the H_2 molecule, a 6×6×1 gamma centered k-point grid is used. The exchange functional is again the original PBE. Cut-off energy as a function of total energy is drawn to figure 4.

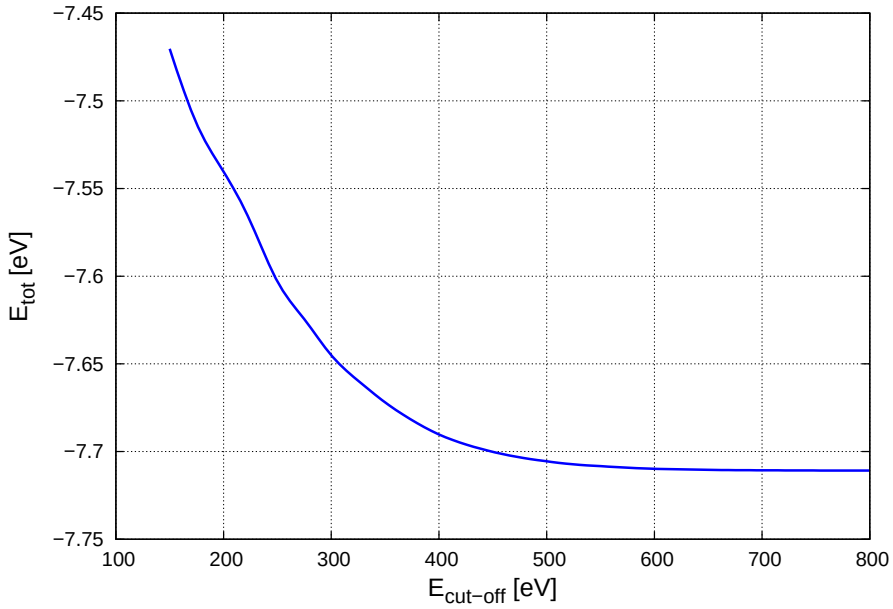

Figure 4: Total energy as a function of cut-off energy for H_2.

Only one cut-off energy can be used in a VASP calculation. In the yet to come adsorption calculations, where several elements are present, the highest cut-off of all elements has to be chosen. In this case, the cut-off energy of H_2 is chosen for adsorption calculations; $E_{\text{cut-off}} = 700$ eV. Again, the same cut-off energy can be chosen for the vdW-DF2 implementation calculation, and calculation without the implementation.

3.1.3 Lattice constants for ruthenium

When relaxing a bulk, a lattice constant, characteristic to that particular solid matter is found. Spin polarized calculations are performed here for Ru. The cut-off energy used here with ruthenium is 400 eV. The exchange correlation functional used in these calculations is the original PBE function [15].

Here ruthenium bulk is allowed to relax. The calculated lattice constants, without employing van der Waals-Density Functional, are $a = 2.73$ Å and $c/a = 1.57$ Å. When using the vdW-DF2 implementation of the VASP code, the following lattice constants are obtained: $a = 2.76$ Å and $c/a = 1.57$ Å, see figures 5 and 6. The experimentally obtained lattice constants for ruthenium are $a = 2.70$ Å, $c/a = 1.59$ Å, and thus, $c = 4.28$ Å [31].

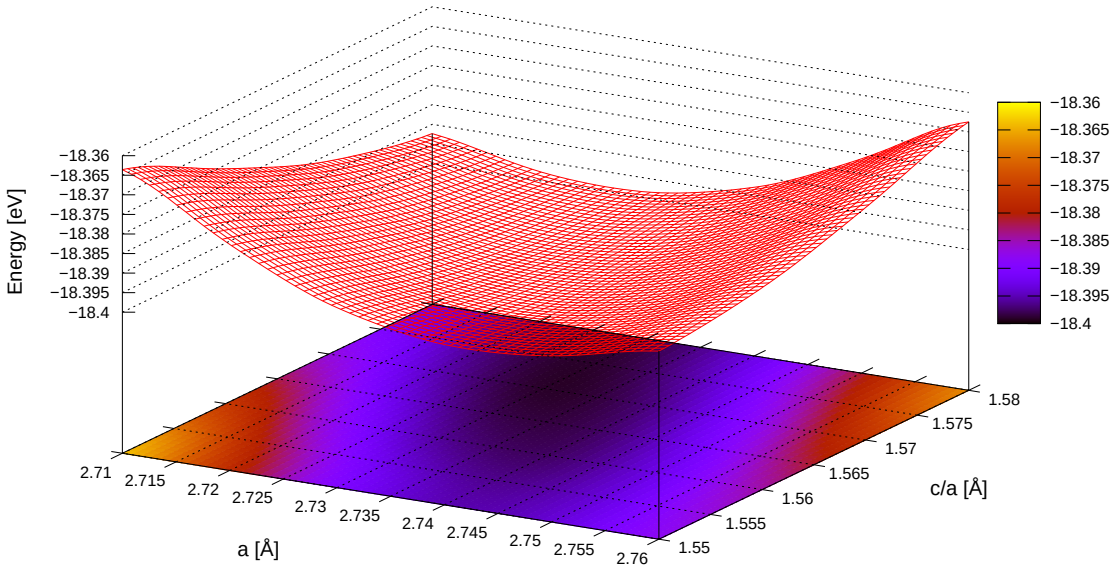

Figure 5: Lattice constants for ruthenium calculated without vdW.

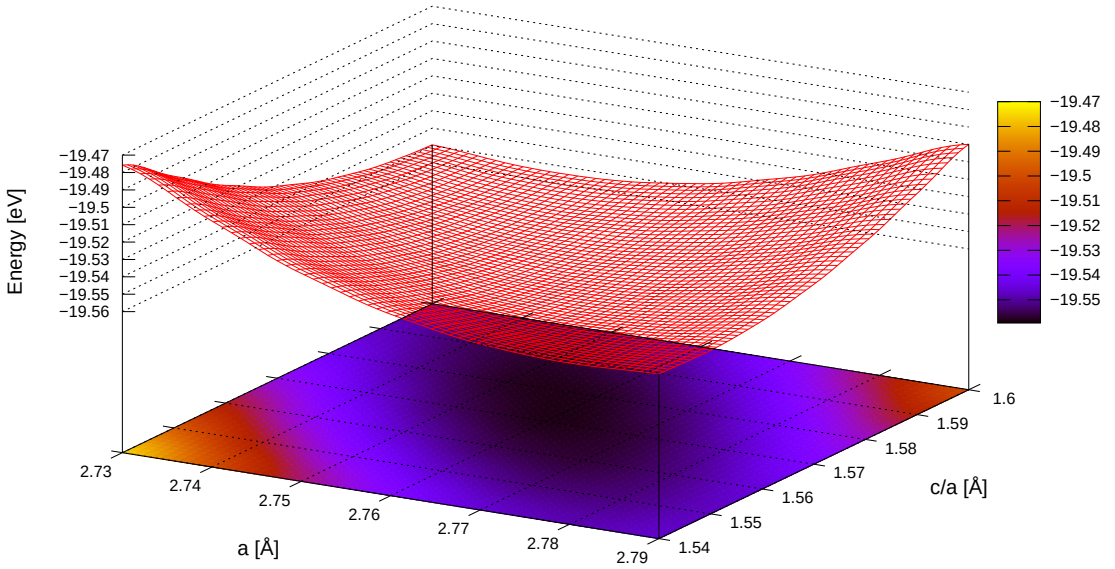

Figure 6: Lattice constants for ruthenium calculated with the vdW-DF2 implementation.

The lattice constants obtained with vdW-DF calculations are larger than the experimentally obtained values. This can be expected based on the vdW-DF method test set calculations by Klimeš *et al.* [6]. The vdW-DF calculations seem to yield larger lattice constants for solids.

3.1.4 H_2 relaxation and vacuum size

When doing calculations with the VASP code, periodic boundary conditions have to be met. Practically said, this is due to the fact that the code reproduces the Bravais lattice in every direction. So, the edges of the user defined Bravais lattice have to have periodic conditions. Hereby it is also clear, that it is crucial to have enough vacuum around a hydrogen molecule, so that it won't "feel" itself in the adjacent Bravais lattice. It would be possible also to increase the H_2 coverage on the surface, but in this study it is not a matter of interest.

In these calculations the cut-off energy of 700 eV is used. A variety of different sized gamma centered k-point grids are tested for the H_2 molecule. The size of $5\times5\times1$ gamma centered grid is found to be the most favorable one for the single hydrogen molecule. PBE PAW potential [26, 27] and the original PBE exchange functional [15] are used within these calculations. Non spin polarized calculations are performed for hydrogen molecule with the VASP code. The optimal vacuum size is determined by focusing on the hydrogen molecule bond length. When the bond length reaches its equilibrium, the vacuum is large enough. The equilibrium bond length and the vacuum size are determined at the same time. The box size and bond length are determined by employing the vdW-DF2 implementation, see figure 7. Results from the corresponding calculation -without employing the vdW-DF2 implementation are shown in figure 8.

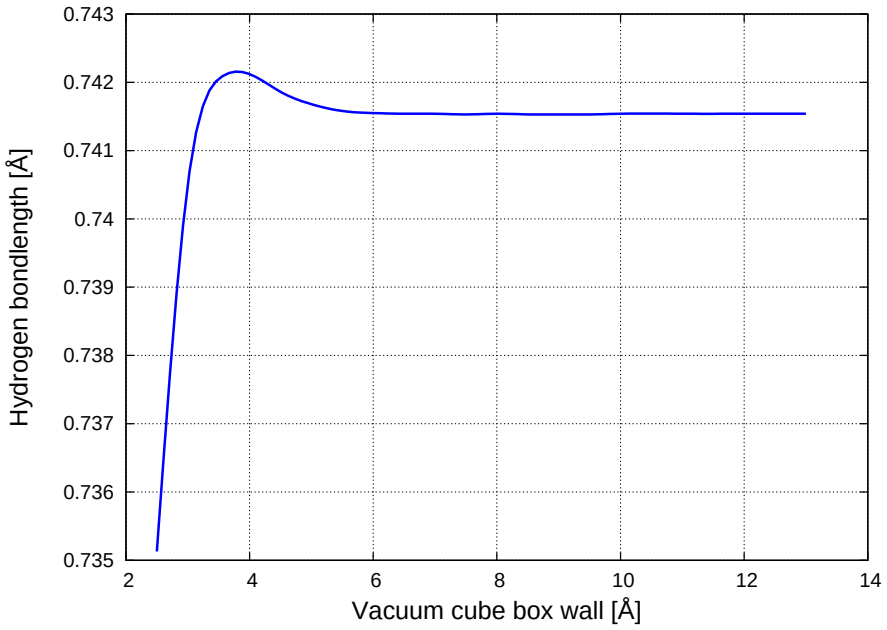

Figure 7: Vacuum box wall sizes (x- and y-directions) and hydrogen bond length calculated with the vdW-DF2 implementation

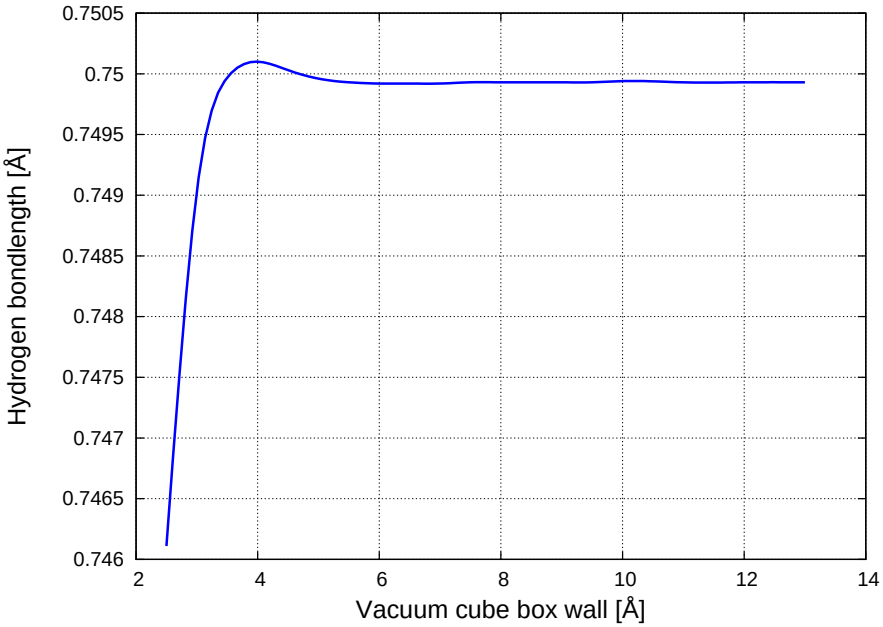

Figure 8: Vacuum box wall sizes (x- and y-directions) and hydrogen bond length calculated without the vdW-DF2.

With the vdW-DF2 implementation, the bond length of H_2 converges to 0.7415 Å. Without the implementation, the corresponding bond length is 0.7499 Å. From the figures 7 and 8 it can be seen how the bond length curve flattens when the vacuum size increases. It can be said that 8 Å of vacuum is sufficient for the hydrogen molecule not to ”feel“ itself in the adjacent Bravais lattice. Also a little less than 8 Å could be enough, but in the end the actual vacuum size in the adsorption calculations will be determined by the hexagonal bulk properties of ruthenium. Also, when planning the adsorption calculations, the H_2 molecule size has to be added to the 8 Å. Only when doing this, it is certain that the molecule won't feel the adjacent Bravais lattice molecule.

3.2 Testing vdW-DF and exchange correlation functionals

Interest to testing exchange functionals alongside the vdW-DF functionals arose from the fact that several new exchange functionals have been presented along the new vdW-DF1 and vdW-DF2 functionals. Same kind of GGA exchange functional testing has already been done, to some extent, but not for ruthenium nor H_2 [6].

A couple of new exchange functionals are introduced recently *e.g.* C09 and PW86R [12, 14]. In this study a set of test calculations is performed for several different correlation functionals -old and new. Calculations are done with the later vdW-DF2 functional [2] and comparison calculations without taking into account the non local correlations *i.e.*,

without employing the vdW-DF2. First the vdW and GGA test calculations are done for one metal, ruthenium. The second section focuses on vdW and GGA testing with H_2 molecule.

3.2.1 Testing vdW-DF and exchange correlation functionals with Ru

In these calculations the original PBE exchange functional [15], revPBE functional [16], PW86 functional [13], and also the following new GGA exchange functionals: PW86R [14] and C09 [12] are tested.

The cohesive energy of a solid is the energy that is needed to break up the solid into isolated atoms. The cohesive energy can be calculated with subtraction of the energy per atom in the bulk and the free atom energy as follows:

$$E_{\text{coh}} = E_{\text{bulk atom}} - E_{\text{free atom}}. \tag{3}$$

Here denoted as $E_{\text{bulk atom}}$, is the energy of a single atom within the ruthenium bulk. $E_{\text{free atom}}$ denotes the energy of a single free Ru atom in a vacuum box. Before the cohesive energy can be determined, these energies have to be calculated separately from one another. Also a proper vacuum size has to be determined for a single ruthenium atom in a box. The size of vacuum is determined, so that the system will not interfere itself when the Bravais lattice is reproduced to every direction by periodic boundary conditions. Also a cut-off energy is calculated to be used with a single Ru atom in vacuum calculations here. Results for these vacuum size and cut-off calculations are shown in figures 9 and 10.

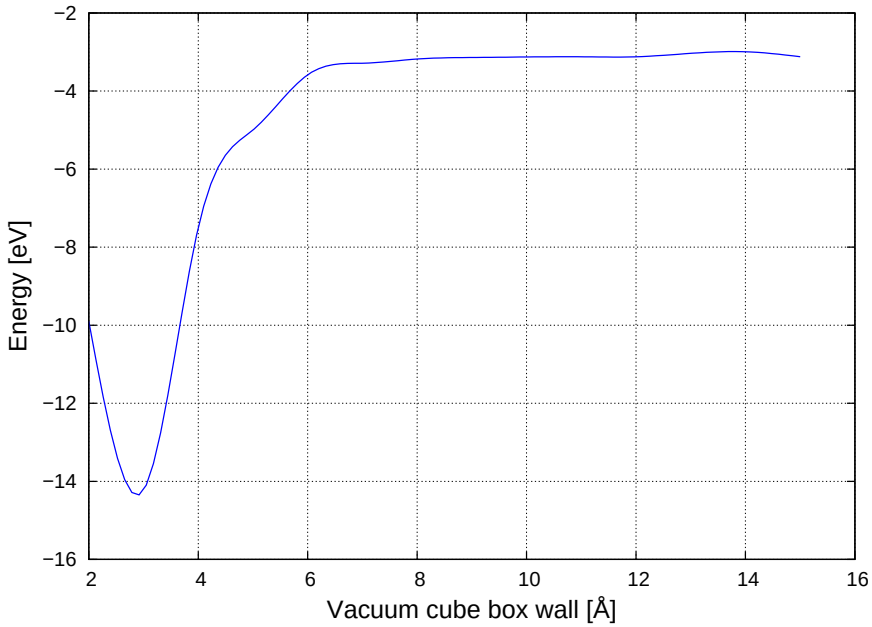

Figure 9: Vacuum size for a single Ru atom.

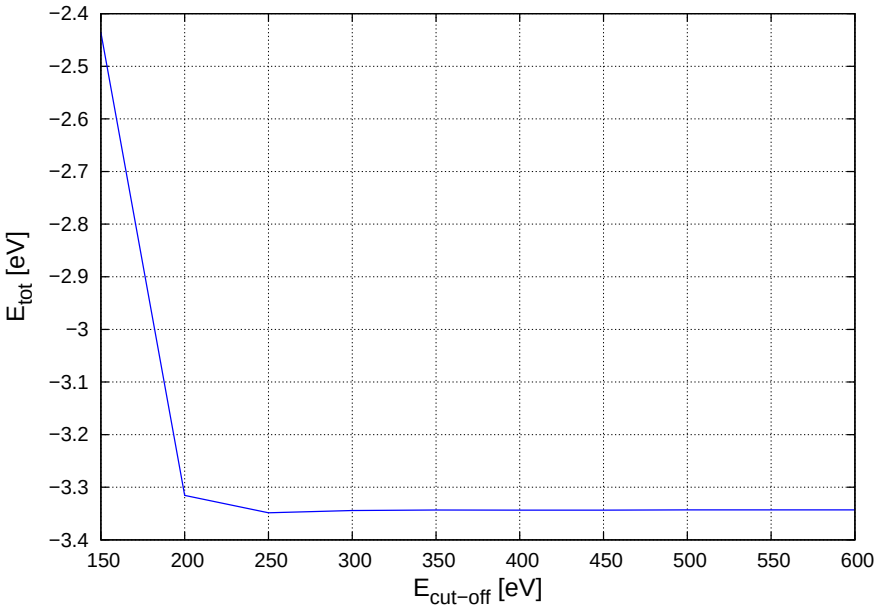

Figure 10: Cut-off for a single Ru atom in a vacuum box.

The cut-off energy of 400 eV can be chosen for the cohesive energy calculation of a single Ru atom. A gamma point only calculation is sufficient for a single Ru atom in a vacuum. Vacuum cube box wall size of 11 Å is enough for the Ru atom not to ”feel“ the adjacent Ru atom.

For bulk ruthenium, a gamma centered (11×11×11) k-point grid is used in cohesive energy calculations. The bulk calculation cut-off energy is 400 eV. All the calculations are done with the vdW-DF2 functional and several different exchange functionals. The calculated lattice constants and cohesive energies are gathered to table 1. The volume of hcp unit triangular prism is calculated here with the motivation that it could be a better comparison parameter than the two lattice constants. Both the volume and the lattice constants are shown in table 1, as well as the cohesive energies.

Table 1: Lattice constants and the volume of hcp unit triangular prism derived from those, as well as the cohesive energies calculated for ruthenium using VASP with vdW-DF2 functional and with different exchange correlation functionals.

Exchange functionals and use of vdW	Ruthenium			
	a [Å]	c/a [Å]	Comparison volume [Å^3]	Cohesive energy [eV]
Experimental	2.70 [31]	1.59 [31]	13.55	-6.68 [32]
PBE vdW-DF2	2.76	1.57	14.29	-6.44
revPBE vdW-DF2	2.77	1.58	14.54	-6.10
PW86 vdW-DF2	2.79	1.58	14.86	-5.65
PW86R vdW-DF2	2.79	1.59	14.95	-5.80
C09 vdW-DF2	2.71	1.58	13.62	-7.69
PBE	2.73	1.57	13.83	-6.85
revPBE	2.74	1.57	13.98	-6.26
PW86	2.77	1.57	14.45	-6.29
PW86R	2.78	1.57	14.61	-6.18
C09	2.69	1.57	13.23	-9.07

The results seem to be consistent with a conclusion of Klimeš *et al.* [6]; the use of vdW functionals produces larger lattice constants (and larger volumes) for solids. It seems as there would be some inverse proportional correlation between the volumes and cohesive energies. The smaller the volume, the larger the cohesive energy. The C09 functional has the smallest volume and the largest cohesive energy, PW86 and PW86R have the largest lattice constants and smallest cohesive energies and the PBE and revPBE seem to be some kind of golden mean here. The C09 functional produces smaller lattice constants than the other functionals, but the cohesive energies seem spuriously large. From the vdW-DF implementation calculations, the original PBE cohesive energy result is the closest to the experimental value, although the cell volume is not the closest.

3.2.2 Testing vdW-DF and exchange correlation functionals with H_2

In these calculations only three of the exchange functionals presented in the previous ruthenium lattice constant and cohesive energy calculations are tested here with the H_2 molecule. The original PBE exchange functional [15] and both of the new functionals PW86R [14] and C09 [12] are considered here.

As stated earlier in this section, when doing calculations with VASP, periodic boundary conditions have to be met. Also, it has to be made sure that there is enough vacuum around the molecule. A hydrogen molecule is placed in a vacuum cube box of 13 Å walls. In these calculations, a $5\times5\times1$ gamma centered k-point grid is used. An appropriate cut-off energy is 700 eV. Non spin polarized calculations are performed for hydrogen with the VASP code. Comparison of different exchange functionals is made here. Also, calculations are done both including van der Waals and without including it.

Table 2: Bond lengths for hydrogen molecule using VASP with vdW-DF2 functional and with different exchange correlation functionals.

Van der Waals and exchange functional	Bond length [Å]
Experimental	0.7414 [33]
PBE vdW-DF2	0.7415
C09 vdW-DF2	0.7529
PW86R vdW-DF2	0.7358
PBE	0.7499
C09	0.7618
PW86R	0.7440

The hydrogen molecule bond lengths are smaller when the vdW-DF functional is used in the calculation. Bond length results seem to favor the use of van der Waals with the original PBE. The PBE vdW-DF2 result is practically equivalent to the experimental value, and the second best result with the vdW-DF2 implementation is obtained with the PW86R. H_2 bond lengths have been calculated earlier with two different exchange functionals by Luppi *et al.* [17]. They used the DACAPO code [34] and the exchange functionals RPBE [35] and PW91 [23]. The non local corrections were not taken into account then. With the RPBE functional they got bond length of 0.755 Å and with the PW91 functional bond length of 0.758 Å. Results are very close to each other with the

two functionals. [17] The results are also quite close to the bond length obtained here with the PBE functional, 0.7499 Å.

The H_2 bond length and the ruthenium lattice constants have different kind of behavior with the vdW-DF2 functional. The ruthenium lattice constants are larger with the non local corrections, but the H_2 bond lengths are smaller with the vdW. Klimes *et al.* stated in their study that the vdW-DF overestimates the lattice constants for solids, ionic solids and semiconductors, while the alkali and alkali-earth lattices are underestimated [6]. The Ru lattice constants here are overestimated, but the H_2 bond length is underestimated only with one of the three exchange correlation functionals. The other two are smaller with the vdW-DF also, but not underestimated.

Disturbingly, the ruthenium lattice constants and the H_2 bond lengths have different kind of behavior with the different exchange functionals. The differences in comparison to the experimental value are not consistent, but vary between with different exchange functionals. Therefore it is quite difficult to draw conclusions on the quality of the particular exchange correlation functional based on comparisons of Ru lattice constants and H_2 bond length. However, the original PBE gave the best cohesive energy in Ru calculations and seemed to be some kind of golden mean among the other exchange functionals. And as said, the PBE vdW-DF2 calculation here yields H_2 bond length practically equivalent to the experimental value. The PBE functional gives good results with both H_2 and Ru; it is the most suitable for this case. Thus, the commonly used original PBE is chosen to be used solely in further calculations.

3.3 Surface calculations

First up in this chapter an appropriate surface cell height for ruthenium is determined. The surface cell has to be thick enough in order to actually represent a surface. A compromise has to be made here between accuracy and computational ability. When a fair thickness is chosen, a suitable k-point grid for that system is determined. After these underlying system configurations, the actual adsorption calculations, meaning the PES calculations can be tackled. The PES calculations give valuable information about the adsorption and dissociation dynamics of the H_2 molecule on the Ru(0001) surface, but also they give information about the role of the vdW-DF and the exchange functionals. In addition to the PES plots, also local density of states (LDOS) plots are created for one adsorption site, the *top* site.

3.3.1 Height of ruthenium surface

After calculating the underlying parameters for ruthenium and H_2, interest turns towards studying the effect of height of the Ru surface to the relaxation results. From 4 to 20 atomic layers high surface cells are reconstructed and relaxed. The 20 layer high surface cell is used here as a sort of a reference. Not only the surface thickness has to be high enough, but it is also crucial to have enough vacuum over the surface in order to actually represent a surface. The vacuum has to be thick enough, that the uppermost Ru atoms can not feel the bottommost atoms in the adjacent Bravais lattice.

In these calculations a $6\times6\times1$ gamma centered k-point grid is used. The appropriate cut-off energy for ruthenium is 400 eV. Spin polarized calculations are performed here for Ru. An adequate vacuum size over the surface is 12 Å.

When speaking about layers in the hexagonal close packed structure, a layer is the group of atoms that have the same z-coordinate. Two bottommost layers are fixed to their initial positions and the rest of the layers are allowed to relax. The first and second layers have to be fixed due to the feature of the computational code of reproducing the Bravais lattice to every direction. After surface cells of all different sizes are relaxed, their relaxed positions are compared to the highest 20 layer surface cell. Precisely the layer height *i.e.*, the distance between two layers is compared. Finally, the height of an uppermost layer is compared to the uppermost layer in the biggest 20 layer surface cell. Correspondingly the next layer from the surface is compared to the next in the 20 layer cell, and so on. Illustrative picture of layer thicknesses is shown in figure 11. The comparisons of layer heights are gathered to table 3.

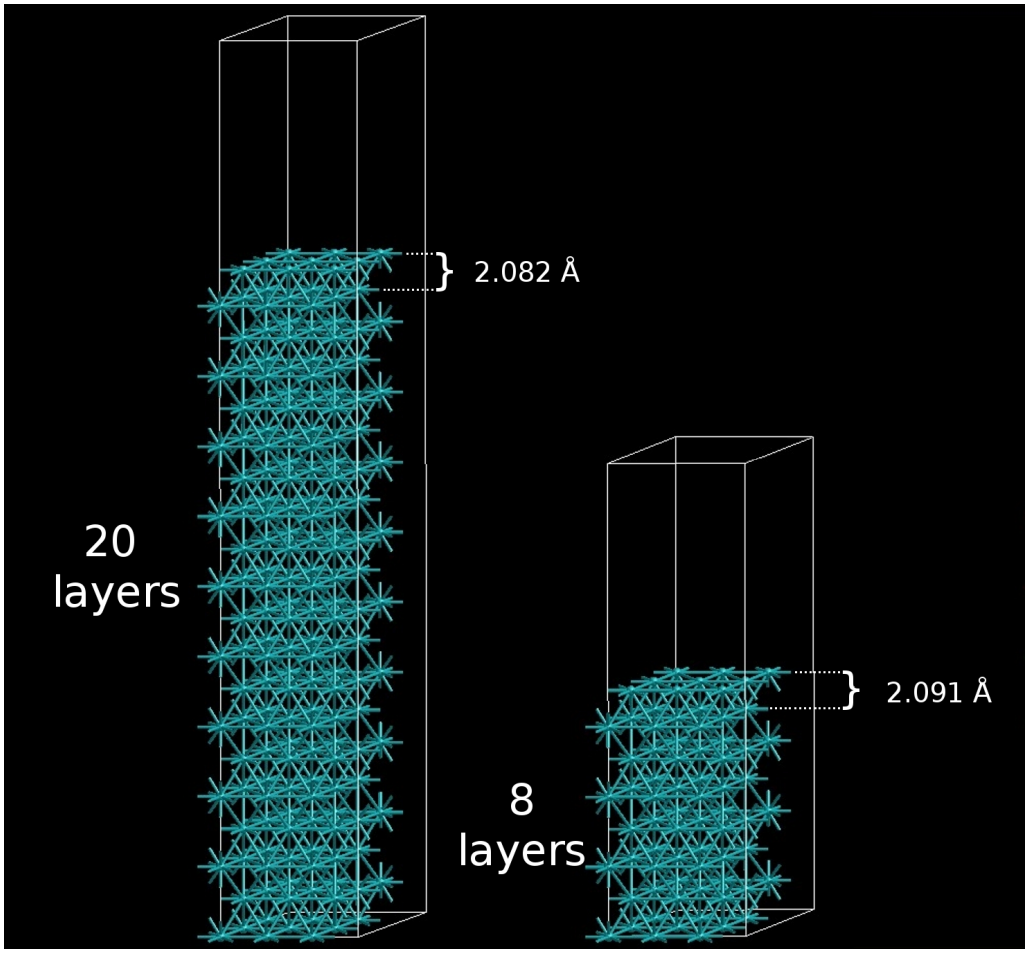

Figure 11: Illustrative figure of ruthenium surface cell thickness. Drawn to the figure are the 20 layers surface cell and the 8 layers surface cell. Thicknesses of the up-most layers are shown in figure. These thicknesses are then compared in order to choose a sufficiently thick surface cell for the adsorption calculations yet to come.

Table 3: Ruthenium surface cell thickness comparison. Differences to the 20 layer surface cell are shown in table.

Surface cell	Surface layers			
	up-most	2. up-most	3. up-most	4. up-most
4 layer high	20-4	19-3	18-2	
	-0.023 Å	0.015 Å	0.004 Å	
6 layer high	20-6	19-5	18-4	17-3
	0.020 Å	-0.011 Å	-0.017 Å	0.022 Å
8 layer high	20-8	19-7	18-6	17-5
	-0.009 Å	0.012 Å	0.004 Å	-0.010 Å
10 layer high	20-10	19-9	18-8	17-7
	0.007 Å	0.004 Å	-0.001 Å	0.007 Å
12 layer high	20-12	19-11	18-10	17-9
	-0.007 Å	0.006 Å	-0.009 Å	-0.003 Å
14 layer high	20-14	19-13	18-12	17-11
	0.007 Å	-0.002 Å	0.002 Å	0.006 Å

When the number of atomic layers increases, consequently the differences to the 20 atomic layer high cell decreases. In the cells from 8 to 14 layers high, the differences of all up-most layers seem to be quite close to each other. Opposed to that, in 4 and 6 layer thick cells the differences increase a notch and also begin to vary even inside the cells. When performing calculations with an *ab initio* computational code, compromises between accuracy and computational cost have to be made from time to time. In the case of surface height, the 8 layer high surface cell is a fair compromise. In 8 atomic layer high surface cell the layers nearest to the surface in comparison to the reference surface cell layers have at the most 0.012 Å difference, and at the smallest 0.004 Å difference. The 8 atomic layer high surface cell is chosen for the potential energy surface calculations yet to come.

3.3.2 K-point testing

The number of k-points influence the accuracy of a calculation. The k-points can be distributed automatically with special k-point grids. Essentially this means that the k-points are distributed homogeneously in the reciprocal unit cell (Brillouin zone). Grids are constructed by the number of subdivisions of the Brillouin zone provided by the user. The higher the number, the more accurate the calculation. For a surface calculation, where

the normal of the surface is perpendicular to z-axis, the z-direction grid parameter should always be one.

In these calculations the size of k-point grid is varied to determine what is the sufficient size for it. Appropriate cut-off energy for ruthenium is 400 eV. Spin polarized calculations are performed here for Ru. An adequate vacuum size over the surface is 11 Å.

Several gamma centered k-point grids are considered here for the 72 atom ruthenium surface cell. Grid sizes are tested to sample the behavior of the accuracy of the calculation. Only gamma centered grids are used for ruthenium, because Ru has a hexagonal close packed (hcp) crystal structure. The Monkhorst-Pack grid is not recommended with the hexagonal crystal structure. Energy converges faster with the gamma centered grids, compared to the Monkhorst-Pack grids when dealing with hexagonal substances. And in fact, the Monkhorst-Pack grids are said not to have full hexagonal symmetry. [30] K-point grids from $2\times2\times1$ to $11\times11\times1$ are tested here. Only even grids from $2\times2\times1$ to $8\times8\times1$ are considered and from there onward odd grids $9\times9\times1$ and $11\times11\times1$. This kind of procedure is recommended in the VASP manual [30]. Energies with the different k-point meshes are plotted in figure 12.

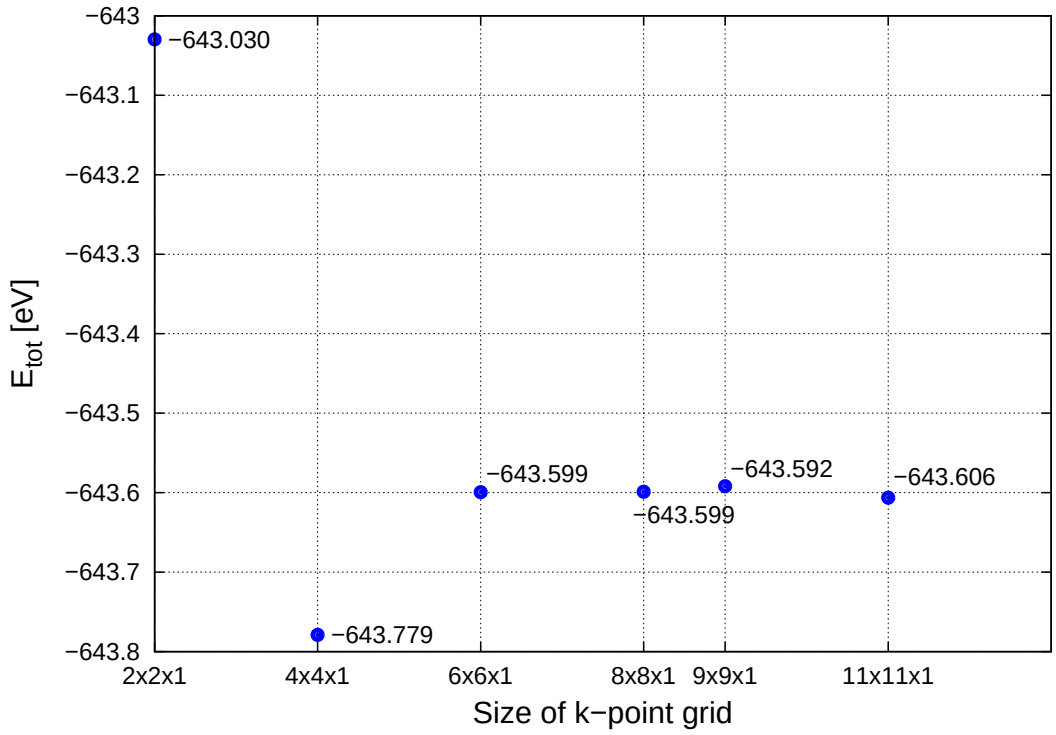

Figure 12: Results for k-point grid calculations from $2\times2\times1$ grid to $11\times11\times1$ grid. Total energies of the 72 atom system are plotted as a function of the k-point grid.

A finding of this test is that the energy seems to converge starting from grid size 6×6×1. It can be concluded from this that 6×6×1 is a sufficient grid size for this particular system. The 6×6×1 gamma centered k-point grid is chosen for further calculations.

3.3.3 Slab relaxation

The 8 atom layer thick ruthenium slab is allowed to relax, with 11 Å vacuum above the slab. The atom positions rearrange from bulk configuration, when they are allowed to relax with the vacuum above the cell. 6×6×1 gamma centered k-point grid is used in these calculations. The cut-off energy is 400 eV.

The slab compresses and the compression of the up-most layer from the bulk position is approximately 0.05 Å. The compression is reasonably small. But this result is in good agreement with the compression result of Luppi *et al.* [17], even though they have used a different slab thickness.

3.3.4 PES calculations

There are four high symmetry adsorption sites in the hexagonal close packed (0001) slab: *top* position, *bridge* position, *fcc* position and *hcp* position. These high symmetry positions will be considered for H_2 adsorption on Ru(0001) surface. Graphical illustration of these positions is shown in figure 13.

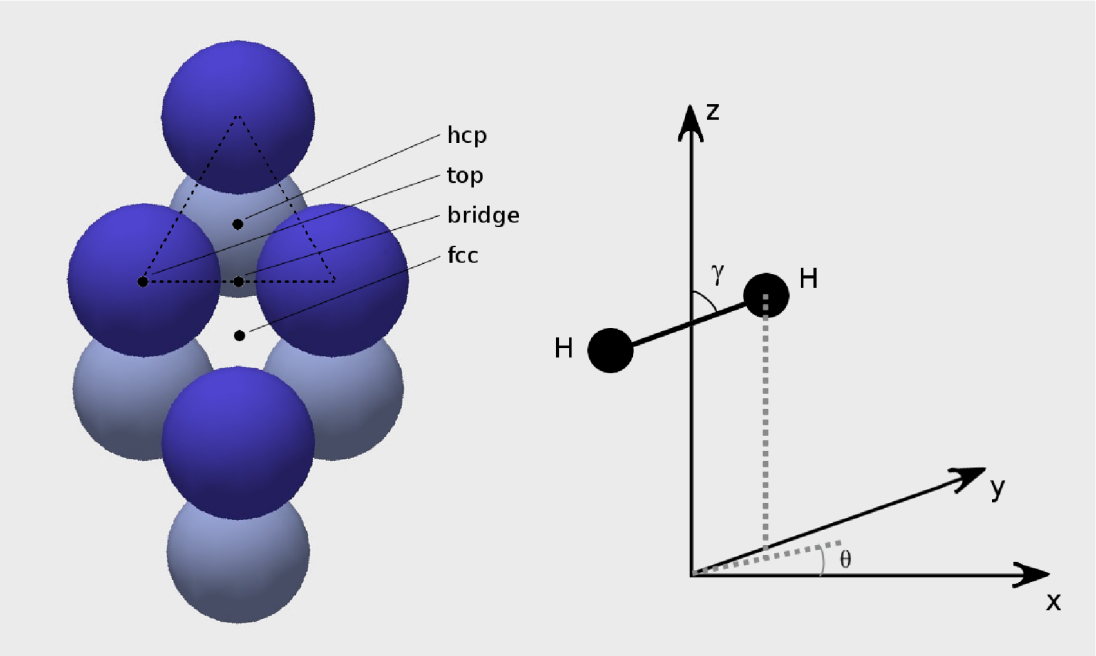

Figure 13: Ruthenium (0001) surface has four high symmetry adsorption sites: *hcp*, *top*, *bridge* and *fcc*. The sites are drawn to the figure on the left. The figure on the right hand side represents rotation and tilt of the H_2 molecule over the particular adsorption site. θ denotes the rotation parallel to the surface and γ denotes the tilt parallel to the normal of the surface. The H_2 molecule sits by its center of mass over the adsorption site.

The exact configurations of the H_2 molecule on the Ru surface in the PES calculations done within this study are presented in figure 14.

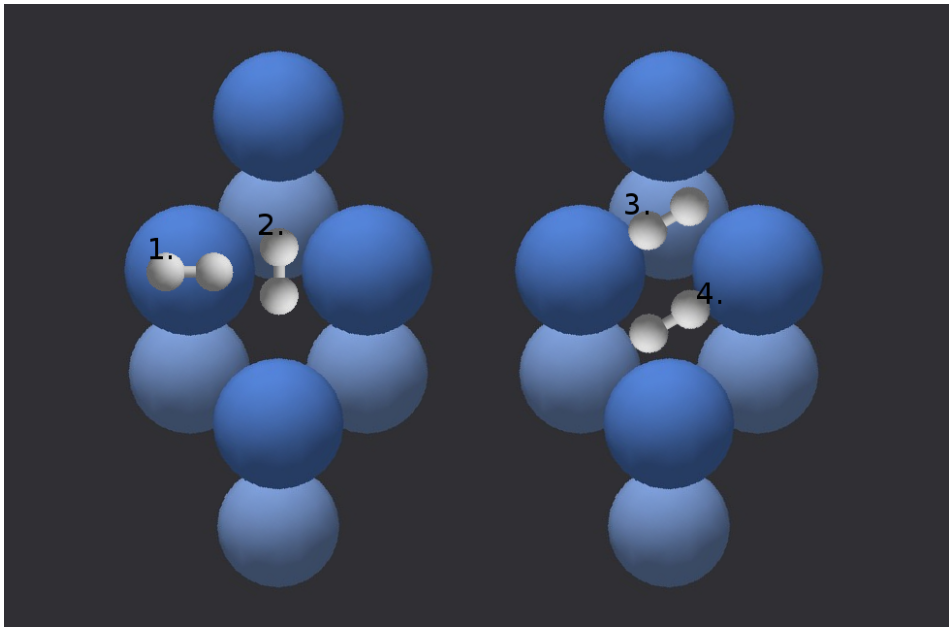

Figure 14: The configurations on adsorption sites are labeled as follows, 1. *top*, 2. *bridge*, 3. *hcp* and 4. *fcc*.

The center of mass of the H_2 molecule is always aligned with the adsorption site. The molecule is parallel to the surface in all four adsorption sites *i.e.* γ is always 90° in these PES calculations. However, the angle θ which denotes the rotation parallel to the surface is not the same in all cases. The H_2 molecule rotates by its center of mass in such a way that for the *top* site $\theta = 0^\circ$, for the *bridge* site $\theta = 90^\circ$ and for the *hcp* and the *fcc* sites $\theta = 30^\circ$. The angles are fixed in the PES calculations and are not allowed to change during the calculation. Luppi *et al.* [17] studied different orientations of the molecule on the Ru surface. They found the orientation parallel to the surface of the H_2 molecule to have the lowest barrier heights, and thus to be the most attractive. Within this study only the orientation parallel to the surface is adopted, as already mentioned.

All of the adsorption sites are covered here with calculations that are done including the vdW-DF implementation of the VASP code and without including it. Luppi *et al.* [17] have presented H_2 on Ru(0001) surface PES plots earlier but without taking the non local corrections into account. To do those calculations they have used a DFT code named DACAPO with ultrasoft pseudopotentials. Luppi *et al.* [17] have used two different exchange functionals in those calculations, the RPBE exchange functional [35] and the PW91 exchange functional [23]. However, in these calculations a different exchange functional is used, the original PBE [15]. The choice of the original PBE is described in the exchange correlation functional testing section above, section 3.2. The PES plots are made with the vdW-DF implementation and without including it to determine the effect of the vdW-DF. And secondly, the effect of the exchange functional to the potential energy surface calculations is evaluated by comparing to the results of Luppi *et al.* [17]. Spin polarized calculations are performed here. The cut-off energy is 700 eV. The k-point grid used here is a gamma centered $6\times6\times1$ grid. 12 Å of vacuum is added above the H_2 molecule in every PES calculation point. Consequently the super cells are of different size. This procedure was undertaken to obtain the same amount of vacuum over the H_2 molecule in every calculation point, and thus to obtain the same conditions for every calculation. In this way one can be sure that the calculation points are comparable with each other.

Note that the PES plots are calculated within some finite limits and therefore one can only state that a particular barrier height has been recorded within the particular study limits. This concerns especially the entrance barrier. Here the entrance channel starts from a very reasonable 3.0-3.5 Å from the surface. As a result of the finite limitation of the entrance channel, one can only state that the entrance barriers are at least as big as the values recorded.

First, the *top* site, that was assumed to be the most reactive of the four is considered. [17] See PES plots of the H_2 approaching the *top* site calculated including the vdW-DF implementation in figure 15 and without including it in figure 16.

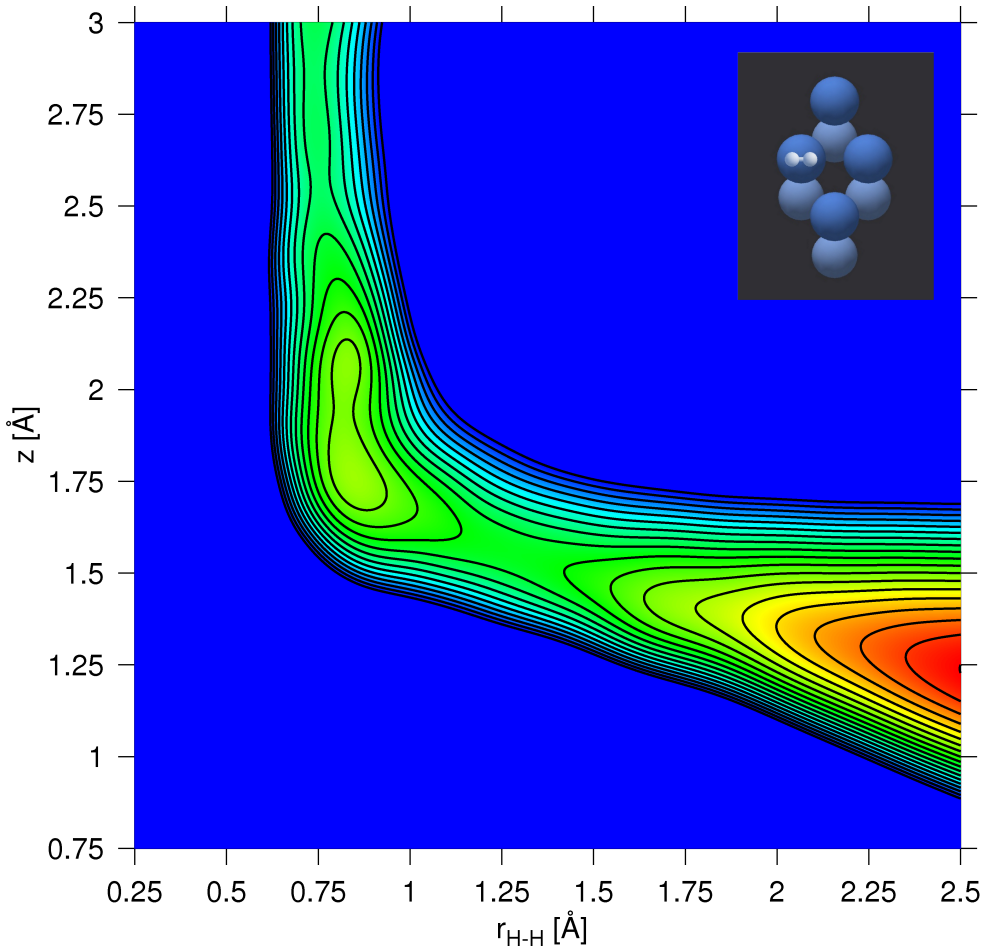

Figure 15: PES for the H_2 approaching the *top* site on Ru(0001), calculated employing the vdW-DF. z denotes the distance between the Ru surface and the H_2 molecule. $r_{\text{H-H}}$ denotes the H_2 bond length. At the *top* site the contour spacing is exceptionally 0.05 eV.

It seems that the surface might be attractive towards the H_2 molecule. There is a barrier of 0.15 eV visible for the dissociation of the molecule.

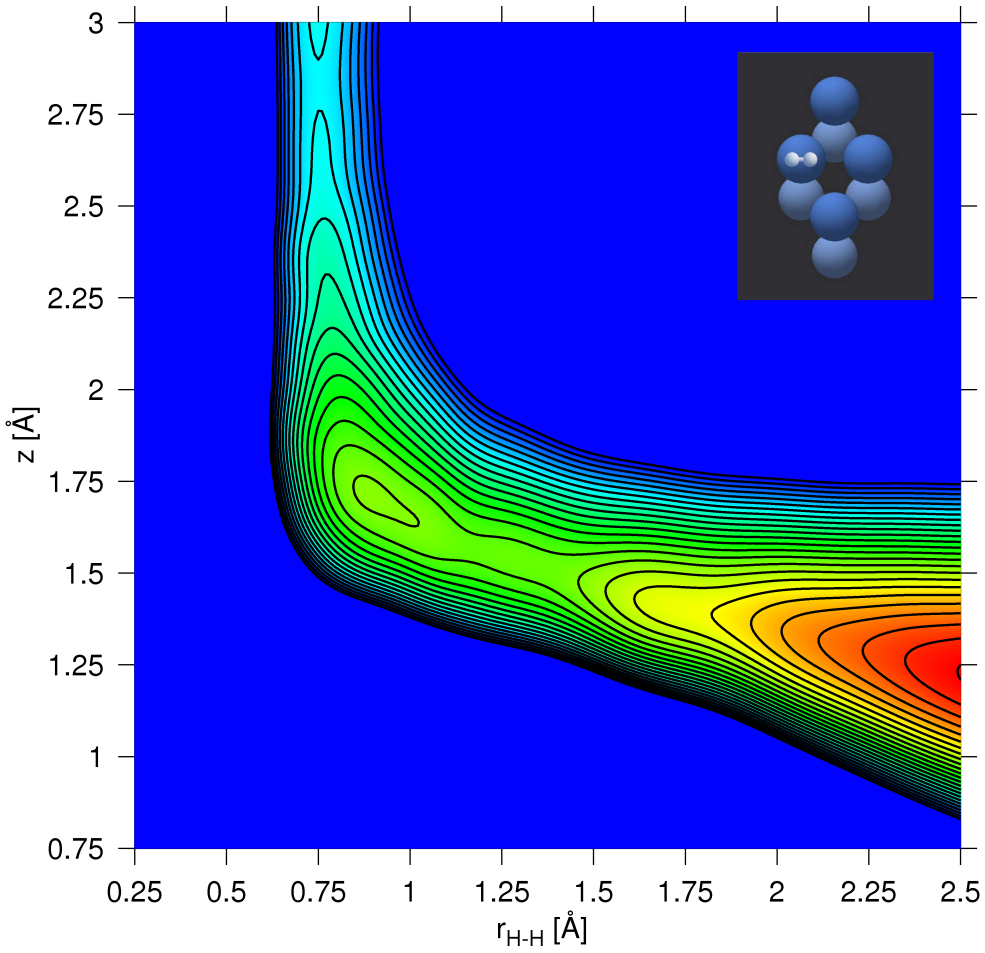

Figure 16: PES for the H_2 approaching the *top* site on Ru(0001), calculated without employing the vdW-DF implementation. z denotes the distance between the Ru surface and the H_2 molecule. $r_{\text{H-H}}$ denotes the H_2 bond length. At the *top* site the contour spacing is exceptionally 0.05 eV.

When calculating without the vdW-DF implementation an entrance barrier seems to occur at the *top* site. The barrier is at least of 0.05 eV high. (The entrance barrier of 0.05 eV is recorded within these evaluation limits.) An entrance barrier was also recorded by Luppi *et al.* [17] with both exchange functionals. With the RPBE they recorded an entrance barrier of 0.085 eV and with the PW91 they recorded a barrier of only 0.013 eV [17]. The result here with the PBE is consistent with the result that Luppi *et al.* [17] got with the RPBE. With the PW91 they recorded a lower entrance barrier.

The calculation here with the vdW-DF though does not record a barrier at the entrance within the accuracy of 0.05 eV. (There is a possibility of a very small barrier, but in any case it falls under the contouring of 0.05 eV.) The calculation done with the vdW-DF implementation indicates that the Ru(0001) *top* site is more attractive towards the H_2 molecule when compared to the calculation made without the vdW-DF.

Neither PES plots indicate spontaneous dissociation of the H_2 molecule. Barrier in the dissociation channel is 0.15 eV for the vdW-DF calculation. For the calculation without the vdW-DF the second channel holds for 0.05 eV barrier (in addition to the barrier of at least 0.05 eV at the entrance channel).

It seems that when the molecule approaches the *top* site, the vdW-DF calculation indicates no entrance barrier (or very fine one) and on the other hand, a stronger dissociation barrier of the H_2 in comparison to the calculation without employing the implementation.

Next, the *bridge* site was considered. See figures 17 and 18 for the H_2 molecule approaching the *bridge* site.

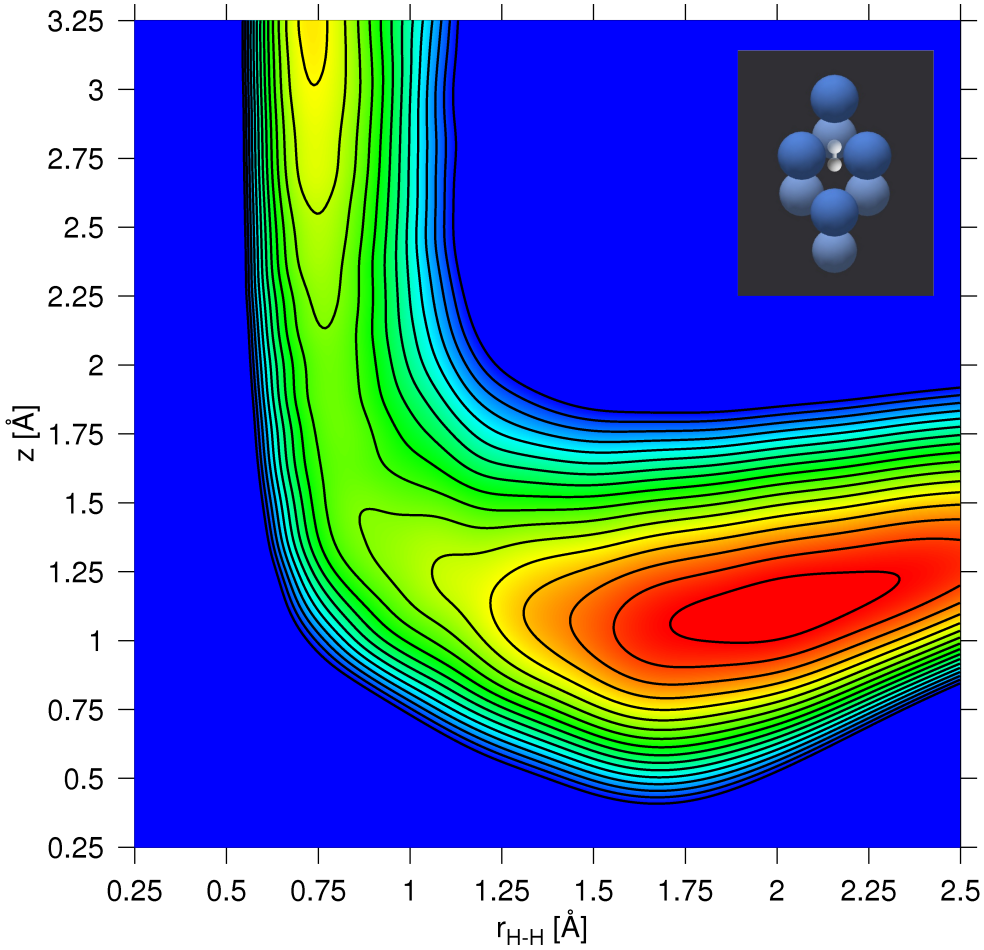

Figure 17: PES for the H_2 approaching the *bridge* site on Ru(0001), calculated employing the vdW-DF. z denotes the distance between the Ru surface and the H_2 molecule. $r_{\text{H-H}}$ denotes the H_2 bond length. The contour spacing is 0.1 eV.

The *bridge* site PES plot, calculated including the vdW-DF implementation indicates a barrier at the entrance channel. However, in close proximity of the Ru surface the H_2 molecule would dissociate. Here, with the vdW-DF the dissociation barrier is at least of 0.3 eV.

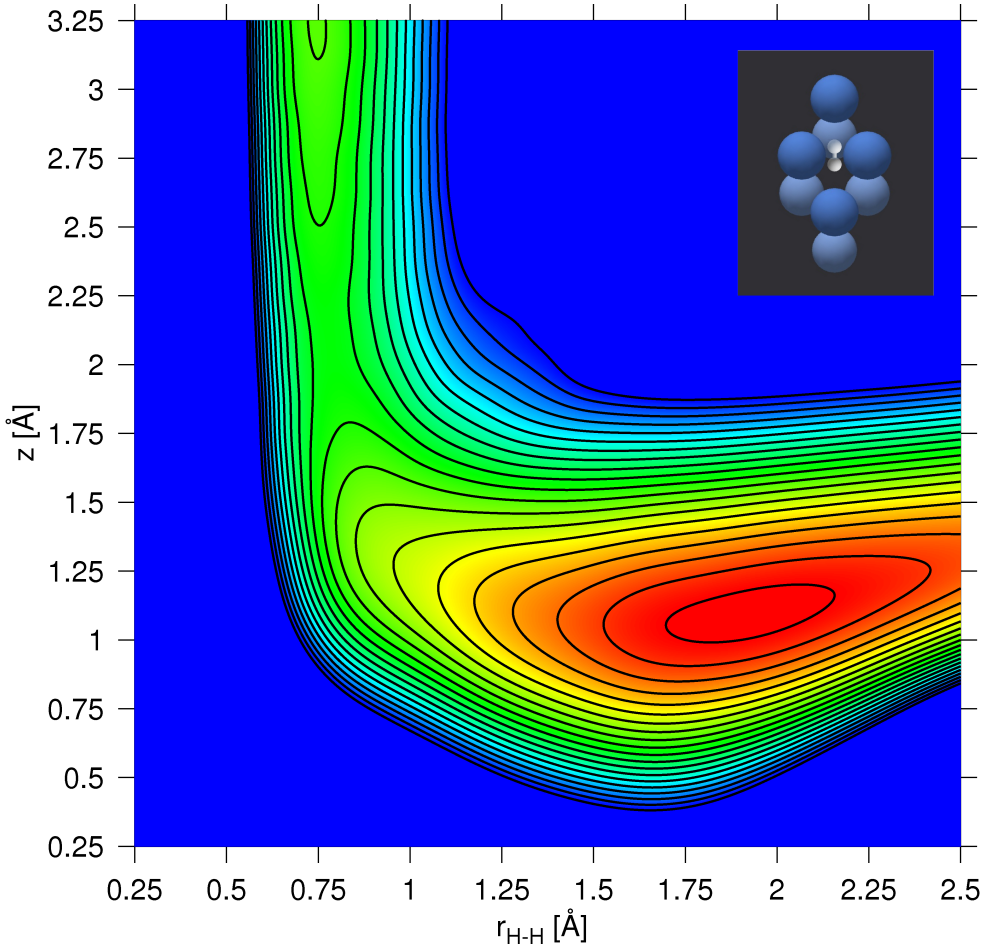

Figure 18: PES for the H_2 approaching the *bridge* site on Ru(0001), calculated without employing the vdW-DF implementation. z denotes the distance between the Ru surface and the H_2 molecule. $r_{\text{H-H}}$ denotes the H_2 bond length. Contour spacing is 0.1 eV

At the *bridge* site the Ru(0001) surface is not attractive. When calculating the *bridge* PES plot without including the vdW-DF implementation, the dissociation barrier seems to be a bit lower, being at least of 0.2 eV. The same trend in the dissociation barriers is recorded for both the *top* and the *bridge* sites, although the surface is more attractive with the vdW-DF, than without it, at the *top* site.

Luppi *et al.* recorded an entrance barrier of 0.333 eV with the RPBE, and with the PW91 they got a barrier of 0.174 eV. At the *bridge* site the result obtained here with the PBE

functional without employing the vdW-DF lies in between the RPBE and PW91 results, being 0.2 eV. [17]

Next, the *fcc* adsorption site at the Ru(0001) surface is considered. See figures 19 and 20 for the H_2 molecule approaching the *fcc* site.

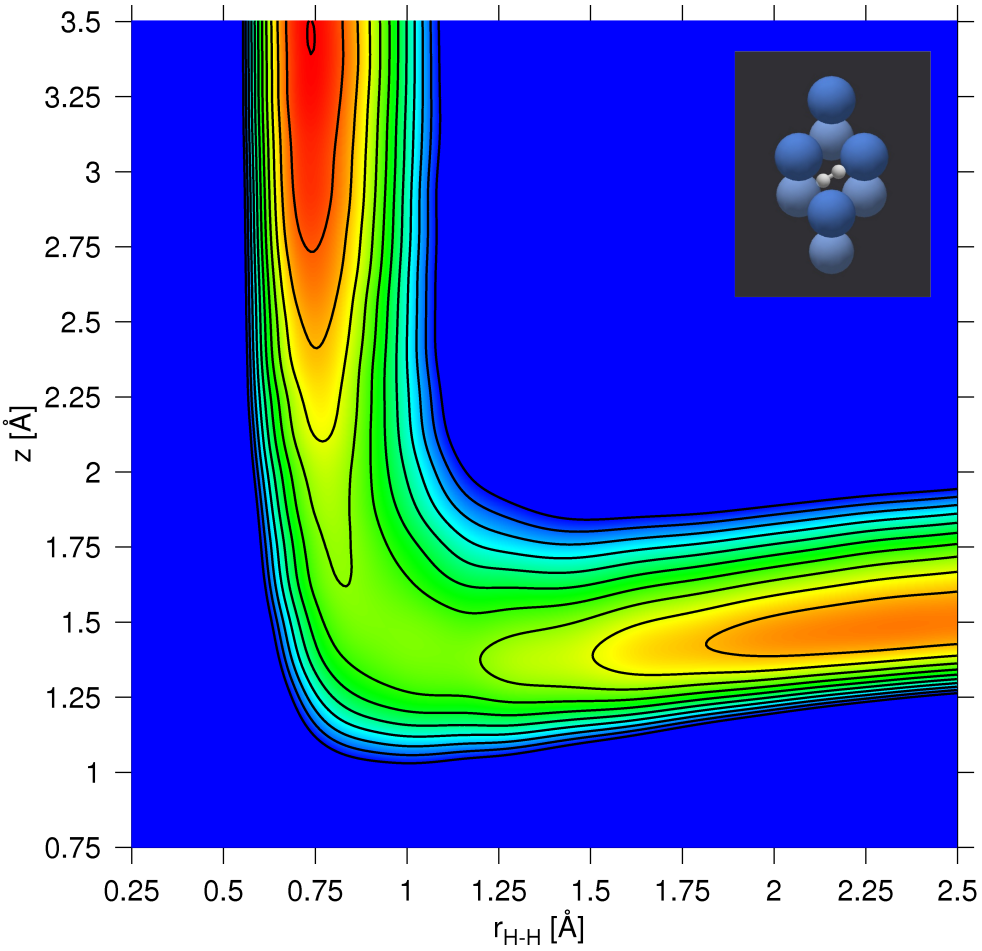

Figure 19: PES for the H_2 approaching the *fcc* site on Ru(0001), calculated employing the vdW-DF. z denotes the distance between the Ru surface and the H_2 molecule. $r_{\text{H-H}}$ denotes the H_2 bond length. The contour spacing is 0.1 eV.

At the *fcc* adsorption site, the surface is not attractive towards the hydrogen molecule. In the calculation with the vdW-DF there exists an entrance barrier of at least 0.5 eV.

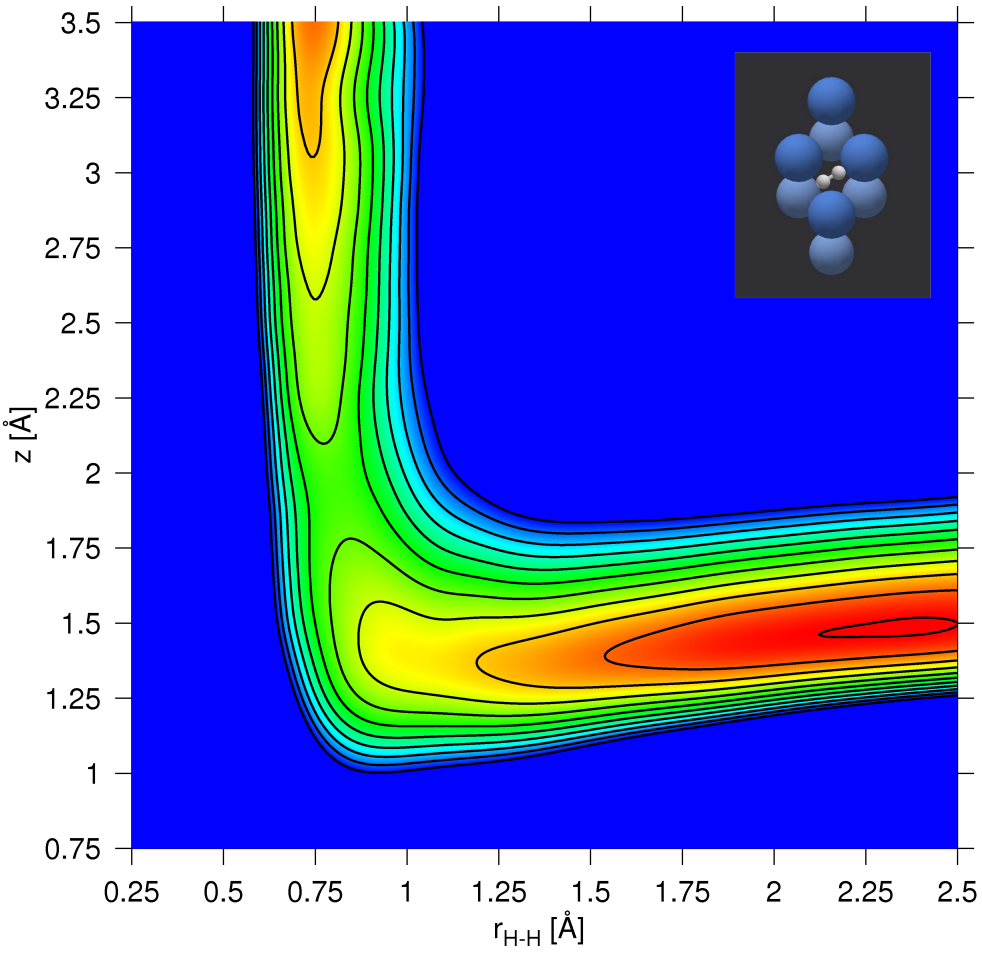

Figure 20: PES for the H_2 approaching the *fcc* site on Ru(0001), calculated without including the vdW-DF implementation. z denotes the distance between the Ru surface and the H_2 molecule. $r_{\text{H-H}}$ denotes the H_2 bond length. The contour spacing is 0.1 eV.

In both calculations, with the the vdW-DF and without it, the surface is not attractive at the *fcc* adsorption site. An entrance barrier of at least 0.3 eV is visible at the *fcc* PES plot without employing the vdW-DF implementation. The entrance barrier is higher in the calculation with employing the vdW-DF implementation. The difference between the two PES calculations is 0.2 eV. Thus the dissociation barrier is again higher with the vdW-DF implementation, as it was at the *top* and the *bridge* sites.

Here, the entrance barrier obtained without the vdW-DF implementation lies again in between the two results that Luppi *et al.* [17] have obtained. They got a 0.436 eV barrier with the RPBE functional, and with the PW91 they got a 0.254 eV barrier. A barrier of 0.3 eV was recorded here without the vdW-DF.

In the last, the *hcp* adsorption site at the Ru(0001) surface is considered. See figures 19 and 20 for the H_2 molecule approaching the *hcp* site.

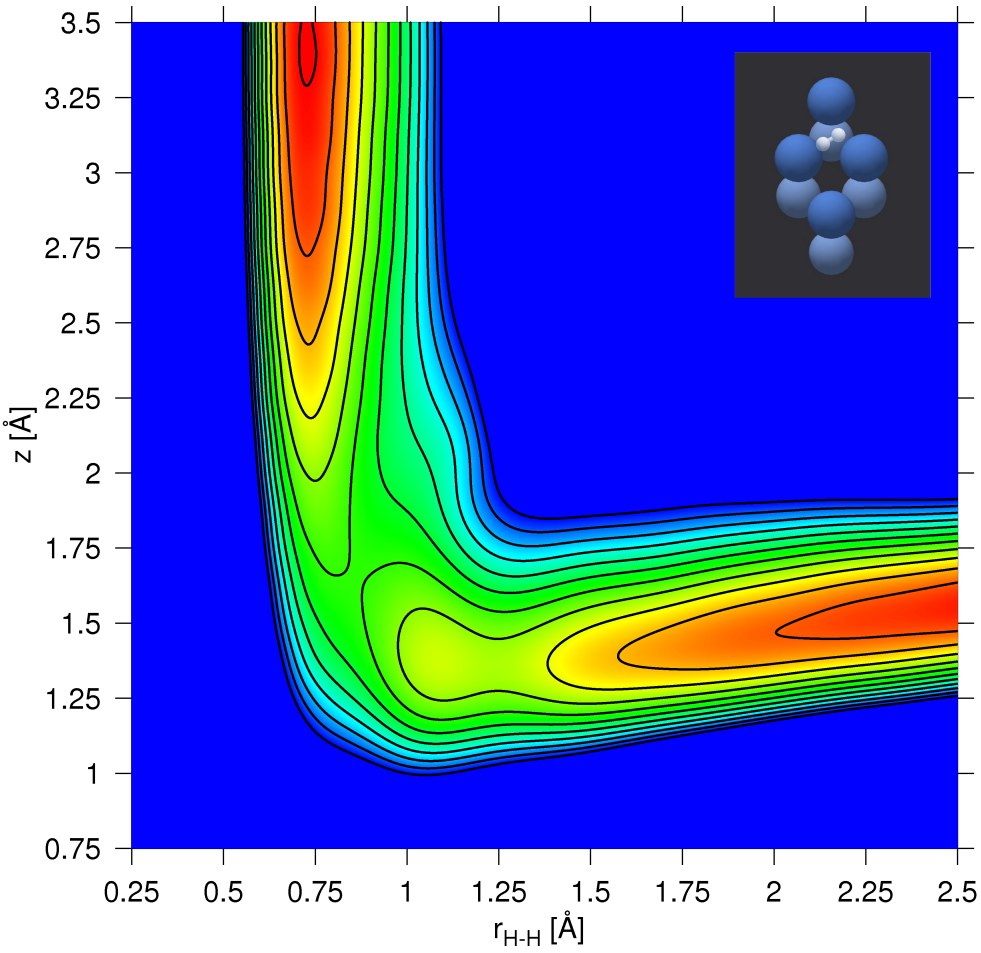

Figure 21: PES for the H_2 approaching the *hcp* site on Ru(0001), calculated employing the vdW-DF. z denotes the distance between the Ru surface and the H_2 molecule. $r_{\text{H-H}}$ denotes the H_2 bond length. Contour spacing is 0.1 eV.

As with the *fcc* adsorption site, the surface is not attractive towards the hydrogen molecule at the *hcp* adsorption site either. Here an entrance barrier of at least 0.6 eV is recorded with the vdW-DF.

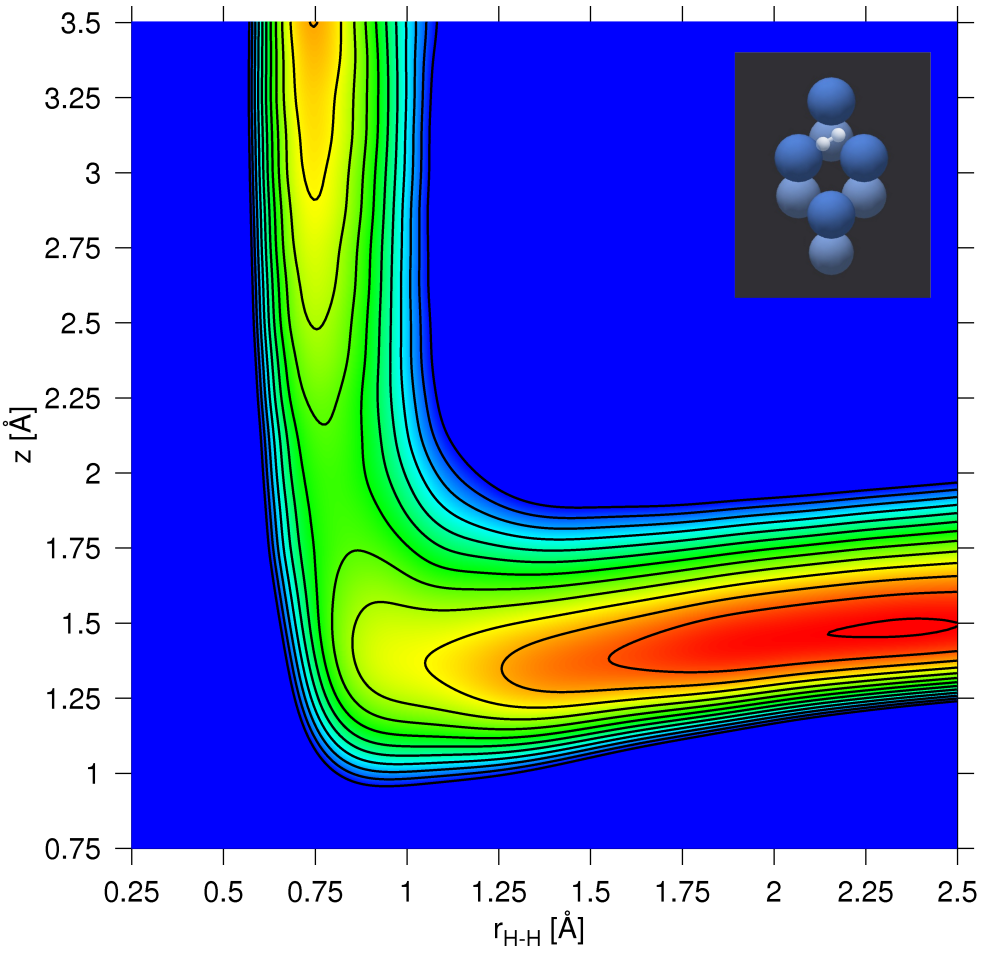

Figure 22: PES for the H_2 approaching the *hcp* site on Ru(0001), calculated without including the vdW-DF implementation. z denotes the distance between the Ru surface and the H_2 molecule. $r_{\text{H-H}}$ denotes the H_2 bond length. Contour spacing is 0.1 eV.

At the *hcp* site the surface is the least attractive of the four adsorption sites studied. Without the vdW-DF at the *hcp* adsorption site there exists an entrance barrier of at least 0.4 eV. This barrier is yet again smaller than with the vdW-DF implementation. Thus, the barrier for dissociation of the H_2 molecule is higher with the vdW-DF.

Luppi *et al.* concluded in their paper, that the *fcc* and *hcp* sites are not significantly different in the regions that are important for the dissociation mechanisms. Therefore the actual *hcp* PESs are not presented in that publication. The *hcp* and *fcc* sites were treated as equivalent. [17] Here the *fcc* and *hcp* sites were studied separately and they are found not to be identical. There is a 0.1 eV difference in the dissociation barrier between the two in both calculations, with the vdW-DF and without it.

Luppi *et al.* have presented results for a few rotated positions, other than those presented within this study. They have obtained heights of dissociation barriers for the following

orientations (in addition to those that have presented in this study also): *top*(θ=90;γ=30), *bridge*(90;45), *bridge*(90;0) and *fcc*/*hcp*(90;0). However, from all the orientations studied, those orientations that are also included in this study yield the lowest barriers for dissociation. [17]

In addition to the high symmetry sites, also one low symmetry adsorption site, the t2f site was studied by Luppi *et al.*, but it is not included into this study at this time. They presented results for three different orientations of the molecule at the t2f site. Tilted orientation t2f(45;50) was found to have the lowest barrier. They also found the t2f site to have the second lowest entrance barrier after the *top* site. [17]

In addition to the *top* site PES plots presented above, also density of states (DOS) plot is created to give further information of the interaction between the H_2 molecule and the Ru surface on the *top* site. The total density of states would include all electrons in the system, but in surface studies one is interested in the bonding process and therefore usually only the electronic orbitals that are directly involved will be considered.

A local density of states (LDOS) plot of H_2 on the *top* site of Ru(0001) surface is presented here. The underlying calculation is made employing the vdW-DF2 implementation. The adsorption calculation, from which the LDOS plot is created, allowed the ruthenium surface atoms to move. Therefore it is not a normal PES calculation, where the surface is "frozen". The nearest Ru atom to the H_2 molecule elevates slightly when the surface atoms are allowed to move. The vdW-DF adsorption calculation gives a 0.852 Å bond length for H_2 and the distance from the center of mass of the molecule to the nearest Ru surface atom is 1.761 Å. Presented in the following figure, figure 23 are the s-DOS for H_2 and d-DOS for the nearest Ru atom.

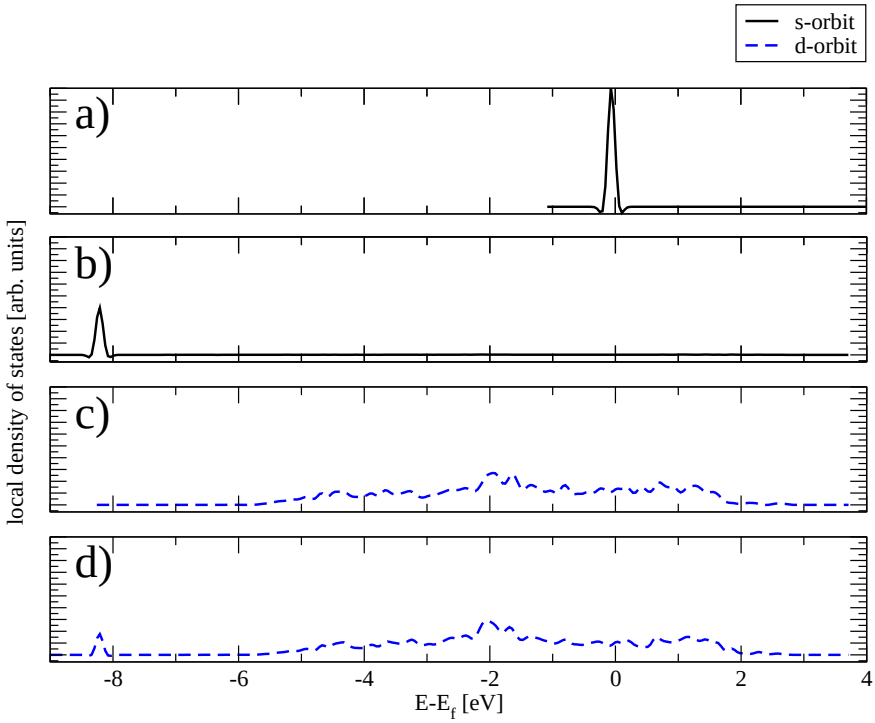

Figure 23: DOS from the vdW-DF adsorption calculation of the H_2 on the *top* site of Ru(0001) surface. a) s-orbit of the H_2 molecule in vacuum, b) s-orbit of the H_2 molecule on the Ru surface, c) d-orbit of the clean Ru surface and d) d-orbit of the nearest Ru to the H_2 on the surface. Figure is created by Mikko Puisto.

There is clear hybridization between H_2 molecule and the nearest Ru atom. Spikes in the sub-figures b) and d) at the same spot indicate bonding.

Information about the H_2 molecule dissociation barriers in *top*, *bridge*, *fcc* and *hcp* sites is gathered to the following table, table 4. The table contains information on the two channels in the adsorption of a diatomic molecule. The entrance barrier E_{Ba} and the second barrier E_{Bb} are given separately. The barrier energies are extracted from the previous PES plots.

Table 4: H_2 on Ru(0001) PES results. All adsorption sites, *top*, *bridge*, *fcc* and *hcp* are covered employing the vdW-DF [2] implementation and without employing it. The original PBE exchange functional [15] is used in these calculations. Dissociation barrier heights are extracted directly from the previous PES plots (figures 15 - 22).

Adsorption site	Use of vdW-DF	Barrier for dissociation	
		Entrance barrier	Second barrier
		E_{Ba} [eV]	E_{Bb} [eV]
Top	with vdW-DF		0.15
	without vdW-DF	0.05	0.05
Bridge	with vdW-DF	0.30	
	without vdW-DF	0.20	
FCC	with vdW-DF	0.50	
	without vdW-DF	0.30	
HCP	with vdW-DF	0.60	
	without vdW-DF	0.40	

The *top* site is the most reactive of the four as was expected. It is visible that the barrier for dissociation of the H_2 molecule is higher at every adsorption site studied here when employing the vdW-DF implementation. Also it is notable, that at the *top* site the vdW-DF calculation predicts no entrance barrier (or very fine one), whereas the calculation where the implementation was not used does. This is the clearest distinction in addition to the higher dissociation barriers in the evaluation of the role of the vdW-DF implementation. Although no entrance barrier was detected within the 0.05 eV marginal at the *top* site with the vdW-DF, the actual barrier for dissociation is nevertheless higher with the implementation. With the vdW-DF the dissociation barrier is 0.15 eV and without the implementation when summing the entrance and the second barriers, the barrier height is 0.10 eV. The vdW-DF seems to bind the H_2 molecule more tightly together and at the *top* site the vdW-DF influences the surface to be more attractive towards the molecule.

Some variance in the heights of the PES barriers when using different exchange correlation functionals was recognized by Luppi *et al.* in their study in 2006. They found the variance to be from 0.072 eV (at the *top* site) to 0.182 eV (at the *fcc*/*hcp* site). [17] Variance was also recorded here, when comparing to the studies of Luppi *et al.* [17], as yet a different exchange functional was employed here, the original PBE [15]. The PBE functional used here yielded results of the entrance barrier in between the two functionals, RPBE and PW91. At the *top* site the calculation with the RPBE and the PBE were

consistent. Otherwise the PW91 predicted the lowest barriers for dissociation, the RPBE predicted the highest and the PBE in the middle.

Luppi *et al.* mentioned in their study that no comparison of complete 6D PESs for different exchange functionals has been attempted before. They see this to be an important aspect within DFT calculations. [17] Within this study some GGA functionals have been compared with Ru lattice constant and cohesive energy and H_2 bond length as the comparison articles. But the usage of PESs as the comparison articles would give more valuable information on the effect of the exchange correlation functionals. However, extensive comparison of different exchange correlation functionals with PESs would be computationally extremely consuming.

3.4 CPU time with the vdW-DF

When using the new vdW-DF2 [2] implementation [11] to the VASP code a question arose of its CPU time demand. Here, evaluation between the calculation times with the vdW-DF and without it is done from the PES data of the previous section, section 3.3.4.

Different adsorption sites *top*, *bridge*, *fcc* and *hcp* are considered individually. The computational times of 580 PES calculation points are used in the comparison between the vdW-DF calculations and the calculations where the non local correlation was omitted. The computational time of one iteration round of finding the electronic ground state energy is used as the evaluation parameter. When using the time of one iteration, the results are comparable between the PES calculation points. The number of iterations is different at each PES point, and thus the use of the time of one iteration is sensible instead of using the total computational time. The PES plots are quite different in different adsorption sites; the sites are considered individually to get more specific information on the CPU time demand. The two calculation sets of one adsorption site are not identical, since the PES plots between the vdW-DF and without it are different by definition. Nevertheless, these CPU time evaluations are done to give a view of the calculation time demand when employing the vdW-DF implementation.

The mean values of computational times from the *top*, *bridge*, *fcc* and *hcp* adsorption sites PES points are calculated. Not the total computational time at each PES point, but the average computational time of one iteration at each PES point. First of all, the mean value for one iteration is derived from the computational time when knowing the number of iterations at each point. Then, the mean value for the time of one iteration at the whole

PES is calculated. Also, standard deviation from the mean is calculated here. The standard deviation yields information on how much the computational time varies between the PES calculation points.

Two different computational platforms were used to do the PES calculations in this study, *i.e.* two different types of hardware and different number of processors were used between the two. Of course, the number of processors at the same platform is invariant in all calculations. The memory limit per processor is the same with both platforms. Naturally, only identical calculations (that are done with the same platform) can be compared with each other. The majority of the PES points are calculated with the same platform, but not all. The other platform is excluded from the evaluation and hence the number of PES points that are considered vary between the adsorption sites.

The mean values for one iteration and the standard deviations are given for all adsorption sites. Furthermore, the change between the vdW-DF calculation and the calculation without employing the implementation is given in percentage. The number of PES points included in the mean value and standard deviation determination is given also. See the results in table 5.

Table 5: Effect of the vdW-DF [2] implementation to the CPU time. PES data from *top*, *bridge*, *fcc* and *hcp* sites is treated individually. Mean value for the computational time of one iteration at each adsorption site is given here. Standard deviation is calculated also. Furthermore, change of the mean between the vdW-DF calculation and the calculation without it is given in percentage.

		Computational time of one iteration	
Ads. site	Use of vdW-DF	Mean [sec] (No. of points)	Standard deviation [sec]
Top	With vdW-DF	397.11 (87)	70.31
	Without vdW-DF	379.04 (83)	61.77
	Change [%]	4.77 % larger with vdW-DF	
Bridge	With vdW-DF	421.76 (102)	68.72
	Without vdW-DF	369.40 (9)	30.43
	Change [%]	14.17 % larger with vdW-DF	
FCC	With vdW-DF	687.60 (78)	119.87
	Without vdW-DF	572.57 (76)	103.30
	Change [%]	20.09 % larger with vdW-DF	
HCP	With vdW-DF	380.93 (76)	91.04
	Without vdW-DF	391.30 (69)	87.66
	Change [%]	2.72 % larger without vdW-DF	

Notable is that the standard deviation is larger with the vdW-DF calculation compared to the calculation without the implementation at all adsorption sites. At the *bridge* adsorption site note that, in calculation without the vdW-DF the number of evaluation points that were able to be used is only 9. Furthermore, the difference between the standard deviations at the *bridge* site is quite large. At all other adsorption sites, the number of evaluation points is quite sufficient for a reliable outcome. The computational time of one iteration round is larger with the vdW-DF at all other adsorption sites except for the *hcp* site. However, at the *hcp* site the difference is the smallest. In there, the computational time without the vdW-DF is only 2.72 % larger than the computational time with the vdW-DF. From *top* to *fcc* sites the vdW-DF computational times are larger by 4.77 % to 20.09 %.

The computational times seem to vary between the adsorption sites, but at the same time the deviations seem to follow the variations. For example, at the *fcc* site the computational times are the largest of the four PESs, but also the deviations are notably larger than at the other sites. The differences in computational times between the PESs and the systematic behavior with the computational times and the deviations is interesting.

4 SUMMARY AND CONCLUSIONS

The role of the van der Waals interactions in the case of H_2 adsorption on Ru(0001) surface is addressed within this study. The vdW-DF2 [2] implementation [11] of the VASP code is employed in the calculations. Alongside the vdW-DF study, the behavior of different exchange functionals is investigated also. At the end, evaluation of the CPU time demand of the vdW-DF is carried out.

4.1 Behavior of vdW-DF and exchange correlation functionals

The role of the vdW-DF2 and the behavior of a few exchange correlation functionals is studied by comparison of H_2 bond lengths and Ru lattice constants and cohesive energies. The H_2 bond length and the ruthenium lattice constants have the opposite behaviors with the vdW-DF2 functional. This is consistent with the conclusion of Klimes *et al.*: the vdW-DF overestimates solids, but the alkali lattices are underestimated [6]. The Ru lattice constants here are overestimated with all exchange functionals studied, and the H_2 bond lengths are also smaller, while actual underestimation occurs with one of the three exchange correlation functionals.

Disturbingly, the ruthenium lattice constants and the H_2 bond lengths have different kind of behavior with the different exchange functionals. The differences to the experimental value are not consistent with each other, but vary between H_2 and Ru with the different functionals. Thus, it is quite difficult to draw conclusions on the quality of the particular exchange correlation functional based on comparisons with the different elements. However, the original PBE exchange functional [15] is picked out as the most suitable for this case and is used solely in further calculations within this study.

In fact, the main source of errors in DFT arises from the approximate nature of the exchange correlation functional E_{xc}. Luppi *et al.* [17] recorded variance in the heights of PES dissociation barriers of H_2 on Ru from 0.072 eV at the *top* site to 0.182 eV at the *fcc/hcp* site when using different exchange correlation functionals. They used the functionals RPBE [35] and PW91 [23]. When comparing the results, the RPBE and the PBE that is employed within this study, are found to be consistent at the *top* site. Otherwise the PW91 predicted the lowest barriers for dissociation, the RPBE predicted the highest and the PBE is in the middle. Luppi *et al.* [17] see that comparison of complete 6D PESs with different exchange functionals might be an important aspect within DFT calculations. However, extensive comparison of different exchange correlation functionals with PESs would be computationally extremely consuming.

4.2 PES calculations and role of vdW-DF

PES plots have been presented for H_2 approaching the Ru(0001) surface at *top*, *bridge*, *fcc* and *hcp* sites employing the vdW-DF2 [2] functional. The vdW functional has not been employed in the case of H_2/Ru before. Corresponding calculations without the implementation were also carried out for comparison. The *top* site is found to be the most reactive of the four. The LDOS plot of H_2 on the *top* site of Ru(0001) surface indicates bonding between the two. The calculations where the vdW-DF is employed yields 0.1 eV - 0.2 eV higher barriers for the dissociation of the H_2 molecule; the vdW-DF seems to bind the H_2 molecule more tightly together. The difference of 0.1 - 0.2 eV in the dissociation barriers is significant. Furthermore, at the *top* site the vdW-DF calculation predicts no entrance barrier (or smaller than 0.05 eV), whereas the calculation where the implementation was not employed does. The difference is not big, but the outcome is substantial if the surface is reactive towards the H_2 molecule with the vdW-DF. This is the clearest distinction in addition to the higher dissociation barriers in evaluation of the role of the vdW-DF implementation in the case of H_2/Ru.

One other adsorption site was studied by Luppi *et al.*, that was not included into this study at this time, the t2f site. They found the site to have the second lowest entrance barrier after the *top* site. [17] It might be interesting to study also the t2f site with including the non local correlations *i.e.*, the vdW-DF functional.

To get information on the different orientations of the H_2 molecule, calculations where the angle θ is not zero, *i.e.* H_2 is not parallel to the Ru(0001) surface could be made. The molecule could be placed for example vertically aligned to the surface. A few rotations of γ however, were investigated by Luppi *et al.* [17], and the orientations that were also used within this paper were found to yield the lowest barriers for dissociation.

To study yet more of the case of H_2 adsorption on the Ru(0001) surface one could carry out calculations, where the molecule would be placed on top of a surface adatom. This case could perhaps be better compared to the experimental results as technically clusters of ruthenium are frequently used in the experimental work to represent the Ru surface.

4.3 CPU time demand of vdW-DF

At the end, the evaluation of the CPU time demand of the vdW-DF2 implementation was made from the PES data. All adsorption sites were studied individually. Computational time of one iteration was used as the evaluation parameter instead of total calculation time.

It is notable that the standard deviation from the mean computational time is larger at all adsorption sites with the vdW-DF implementation. Furthermore, the mean values for the computational time per one iteration are larger with the vdW-DF at all other adsorption sites, except at the *hcp* site. There it was slightly larger without the vdW-DF by 2.72 %. From *top* to *fcc* sites the computational time demand is larger by 4.77 % to 20.09 % with the vdW-DF.

The computational times seem to vary between the PESs, but at the same time the deviations seem to follow the variations. For example, at the *fcc* site the computational times are the largest of the four PESs, but also the deviations are notably larger than at the other sites. This behavior is interesting and leads to contemplating upon how the CPU time demand evaluation could be addressed.

References

[1] M. Dion, H. Rydberg, E. Schröder, D. C. Langreth, and B. I. Lundqvist, "Van der Waals Density Functional for General Geometries," *Phys. Rev. Lett.*, vol. 92, p. 246401, Jun 2004.

[2] K. Lee, É. D. Murray, L. Kong, B. I. Lundqvist, and D. C. Langreth, "A higher-accuracy van der Waals density functional," *Phys. Rev. B*, vol. 82, p. 081101, Aug 2010.

[3] M. Mura, A. Gulans, T. Thonhauser, and L. Kantorovich, "Role of van der waals interaction in forming molecule-metal junctions: flat organic molecules on the Au(111) surface," *Phys. Chem. Chem. Phys.*, vol. 12, pp. 4759–4767, 2010.

[4] J. Blomqvist and P. Salo, "First-principles study for the adsorption of segments of BPA-PC on α-Al_2O_3(0001)," *Phys. Rev. B*, vol. 84, p. 153410, Oct 2011.

[5] D. C. Langreth, B. I. Lundqvist, S. D. Chakarova-Käck, V. R. Cooper, M. Dion, P. Hyldgaard, A. Kelkkanen, J. Kleis, L. Kong, S. Li, P. G. Moses, E. Murray, A. Puzder, H. Rydberg, E. Schröder, and T. Thonhauser, "A density functional for sparse matter," *Journal of Physics: Condensed Matter*, vol. 21, no. 8, p. 084203, 2009.

[6] J. Klimeš, D. R. Bowler, and A. Michaelides, "Van der Waals density functionals applied to solids," *Phys. Rev. B*, vol. 83, p. 195131, May 2011.

[7] G. Kresse and J. Hafner, "*Ab initio* molecular dynamics for liquid metals," *Phys. Rev. B*, vol. 47, pp. 558–561, Jan 1993.

[8] G. Kresse and J. Hafner, "*Ab initio* molecular-dynamics simulation of the liquid-metal–amorphous-semiconductor transition in germanium," *Phys. Rev. B*, vol. 49, pp. 14251–14269, May 1994.

[9] G. Kresse and J. Furthmüller, "Efficiency of ab-initio total energy calculations for metals and semiconductors using a plane-wave basis set," *Computational Materials Science*, vol. 6, pp. 15 – 50, Jul 1996.

[10] G. Kresse and J. Furthmüller, "Efficient iterative schemes for *ab initio* total-energy calculations using a plane-wave basis set," *Phys. Rev. B*, vol. 54, pp. 11169–11186, Oct 1996.

[11] A. Gulans, M. J. Puska, and R. M. Nieminen, "Linear-scaling self-consistent implementation of the van der Waals density functional," *Phys. Rev. B*, vol. 79, p. 201105, May 2009.

[12] V. R. Cooper, "Van der Waals density functional: An appropriate exchange functional," *Phys. Rev. B*, vol. 81, p. 161104, Apr 2010.

[13] J. P. Perdew and W. Yue, "Accurate and simple density functional for the electronic exchange energy: Generalized gradient approximation," *Phys. Rev. B*, vol. 33, pp. 8800–8802, Jun 1986.

[14] É. D. Murray, K. Lee, and D. C. Langreth, "Investigation of exchange energy density functional accuracy for interacting molecules," *Journal of Chemical Theory and Computation*, vol. 5, pp. 2754–2762, Sep 2009.

[15] J. P. Perdew, K. Burke, and M. Ernzerhof, "Generalized Gradient Approximation Made Simple," *Phys. Rev. Lett.*, vol. 77, pp. 3865–3868, Oct 1996.

[16] Y. Zhang and W. Yang, "Comment on "Generalized Gradient Approximation Made Simple"," *Phys. Rev. Lett.*, vol. 80, pp. 890–890, Jan 1998.

[17] M. Luppi, R. A. Olsen, and E. J. Baerends, "Six-dimensional potential energy surface for H_2 at Ru(0001)," *Phys. Chem. Chem. Phys.*, vol. 8, pp. 688–696, 2006.

[18] P. Hohenberg and W. Kohn, "Inhomogeneous Electron Gas," *Phys. Rev.*, vol. 136, pp. B864–B871, Nov 1964.

[19] W. Kohn and L. J. Sham, "Self-Consistent Equations Including Exchange and Correlation Effects," *Phys. Rev.*, vol. 140, pp. A1133–A1138, Nov 1965.

[20] R. Martin, *Electronic Structure: Basic Theory and Practical Methods*. Cambridge University Press, 2004.

[21] D. C. Langreth and M. J. Mehl, "Beyond the local-density approximation in calculations of ground-state electronic properties," *Phys. Rev. B*, vol. 28, pp. 1809–1834, Aug 1983.

[22] A. D. Becke, "Density-functional exchange-energy approximation with correct asymptotic behavior," *Phys. Rev. A*, vol. 38, pp. 3098–3100, Sep 1988.

[23] J. P. Perdew, J. A. Chevary, S. H. Vosko, K. A. Jackson, M. R. Pederson, D. J. Singh, and C. Fiolhais, "Atoms, molecules, solids, and surfaces: Applications of the generalized gradient approximation for exchange and correlation," *Phys. Rev. B*, vol. 46, pp. 6671–6687, Sep 1992.

[24] J. M. Shi, F. M. Peeters, G. Q. Hai, and J. T. Devreese, "Erratum: Donor transition energy in GaAs superlattices in a magnetic field along the growth axis," *Phys. Rev. B*, vol. 48, pp. 4978–4978, Aug 1993.

[25] V. G. Ruiz, W. Liu, E. Zojer, M. Scheffler, and A. Tkatchenko, "Density-functional theory with screened van der waals interactions for the modeling of hybrid inorganic-organic systems," *Phys. Rev. Lett.*, vol. 108, p. 146103, Apr 2012.

[26] P. E. Blöchl, "Projector augmented-wave method," *Phys. Rev. B*, vol. 50, pp. 17953–17979, Dec 1994.

[27] G. Kresse and D. Joubert, "From ultrasoft pseudopotentials to the projector augmented-wave method," *Phys. Rev. B*, vol. 59, pp. 1758–1775, Jan 1999.

[28] P. Blöchl, C. Först, and J. Schimpl, "Projector augmented wave method: *ab initio* molecular dynamics with full wave functions," *Bulletin of Materials Science*, vol. 26, pp. 33–41, Jan 2003. 10.1007/BF02712785.

[29] M. Lahti, A. Puisto, M. Alatalo, and T. Rahman, "The role of preadsorbed sulphur and oxygen in O_2 dissociation on Pd(100)," *Surface Science*, vol. 602, no. 24, pp. 3660–3666, 2008.

[30] G. Kresse, M. Marsman, and J. Furthmüller, "VASP the GUIDE." urlhttp://cms.mpi.univie.ac.at/vasp/vasp/vasp.html. Accessed: 9.1.2012.

[31] N. W. Ashcroft and N. D. Mermin, *Solid State Physics*. Holt-Saunders International Editions: Science : Physics, United States of America: Thomson Learning, 1976.

[32] J. Sólyom, *Fundamentals of the Physics of Solids*. No. vol. 2 in Fundamentals of the Physics of Solids, Springer, 2007.

[33] P. Atkins and J. Paula, *Atkins' Physical Chemistry*. Oxford University Press, seventh Edition ed., 2002.

[34] "Dacapo." urlhttps://wiki.fysik.dtu.dk/dacapo. Accessed: 27.9.2012.

[35] B. Hammer, L. B. Hansen, and J. K. Nørskov, "Improved adsorption energetics within density-functional theory using revised Perdew-Burke-Ernzerhof functionals," *Phys. Rev. B*, vol. 59, pp. 7413–7421, Mar 1999.